Published in final edited form as:

J Comp Neurol. 2022 August ; 530(12): 2154–2175. doi:10.1002/cne.25325.

Integrated age-related immunohistological changes occur in human olfactory epithelium and olfactory bulb

Mira Fitzek[1,2],

Parthkumar K. Patel[2],

Peter D. Solomon[2],

Brian Lin[2],

Thomas Hummel[1],

James E. Schwob[2],

Eric H. Holbrook[2,3]

[1]Smell and Taste Clinic, Department of ORL, TU Dresden, Dresden, Germany

[2]Department of Developmental, Molecular, and Chemical Biology, Tufts University School of Medicine, Boston, MA, United States

[3]Department of Otolaryngology-Head and Neck Surgery, Harvard Medical School, Massachusetts Eye and Ear, Boston, MA, United States

Abstract

Olfactory epithelium (OE) is capable of lifelong regeneration due to presence of basal progenitor cells that respond to injury or neuronal loss with increased activity. However, this capability diminishes with advancing age and a decrease in odor perception in older individuals is well established. To characterize changes associated with age in the peripheral olfactory system, an in-depth analysis of the OE and its neuronal projections onto the olfactory bulb (OB) as a function of age was performed. Human olfactory tissue autopsy samples from 36 subjects with an average age of 74.1 years were analyzed. Established cell type-specific antibodies were used to identify OE component cells in whole mucosal sheets and epithelial sections as well as glomeruli and periglomerular structures in OB sections. With age, a reduction in OE area occurs across the mucosa progressing in a posterior-dorsal direction. Deterioration of the olfactory system is accompanied with diminution of neuron-containing OE, mature OSNs and OB innervation. On an individual level, the neuronal density within the epithelium appears to predict synapse

*CORRESPONDENCE TO: Dr. Eric H. Holbrook, Department of Otolaryngology, Massachusetts Eye and Ear, 243 Charles Street, Boston, MA 02114, eric_holbrook@meei.harvard.edu.

AUTHOR CONTRIBUTIONS

Conceptualization: J.E.S. and E.H.H.; Histology and imaging: M.F., P.K.P., P.D.S., and E.H.H.; Data analysis: M.F., P.K.P., B.L., J.E.S, and E.H.H.; Writing—original draft: M.F., J.E.S., and E.H.H.; Writing—review and editing: all authors; Funding acquisition: J.E.S.

CONFLICT OF INTEREST STATEMENT: The authors declare they have no conflicts of interest.

ETHICS APPROVAL STATEMENT: All procedures performed in studies involving human participants were in accordance with the ethical standards of the institutional and/or national research committee and with the 1964 Helsinki declaration and its later amendments or comparable ethical standards.

PATIENT CONSENT STATEMENT: For this type of study formal consent was not required and the study was considered exempt by the Massachusetts Eye and Ear IRB.

density within the OB. The innervation of the OB is uneven with higher density at the ventral half that decreases with age as opposed to stable innervation at the dorsal half. Respiratory metaplasia, submucosal cysts and neuromata, were commonly identified in aged OE. The finding of respiratory metaplasia and aneuronal epithelium with reduction in global basal cells suggests a progression of stem cell quiescence as an underlying pathophysiology of age-related smell loss in humans.

Graphical Abstract

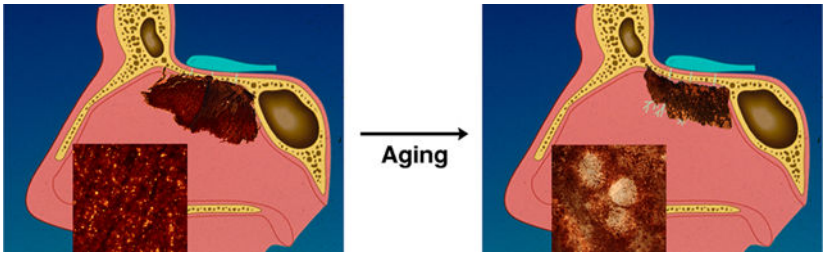

During human development a complete uninterrupted sheet of neuronal competent mucosa with well demarcated boarders comprises the olfactory epithelium (OE) within the superior aspect of the nasal cavity along the septum and lateral wall. The olfactory neurons target in individual glomeruli along the peripheral edges of the olfactory bulb (OB). With advancing age, regions of the OE are disrupted and replaced with respiratory or aneuronal epithelium while the boarder becomes less defined. A decreasing area of OE occurs with a shift of neuronal density in a more posterior-dorsal direction. Intraepithelial neuromas and subepithelial cysts develop along with a decrease in olfactory sensory neurons (OSNs). Proximally, distortions in olfactory targeting occur within the OB with an overall reduction in synapses in the ventral portion.

Keywords

horizontal basal cells; globose basal cells; neuronal aging; autopsy; immunofluorescence; whole mount staining; OMP

INTRODUCTION

Our current understanding of the anatomy of the human olfactory epithelium (OE) and olfactory bulb (OB) has been growing steadily in recent years due to advances in molecular and immunohistochemical techniques. The structure of human OE and constituent cells including surface marker and transcription factor expression closely resembles that described in rodents (Holbrook et al. 2011; Nakashima et al. 1991; Morrison and Costanzo 1992). Located in the upper nasal cavity inferior to the cribriform plate and lining the upper septum and middle/superior turbinate, the OE is composed of three main cell types: 1) microvillar-capped supporting cells extending from the basal lamina to the epithelial surface, 2) multiple layers of olfactory sensory neurons (OSNs) located in the middle of the epithelium with the general progression from more immature cells basally to more mature cells apically, and 3) basal cells near the basal lamina including horizontal basal cells (HBCs) - the reserve stem cell population that is called upon to regenerate all cells

of the epithelium under severe injury, and global basal cells (GBCs) - sitting apical to the HBCs and responsible for the normal homeostatic maintenance of the olfactory neuronal population (Holbrook et al. 2011; Nakashima et al. 1991; Morrison and Costanzo 1992; de Lorenzo 1957; Huard et al. 1998). The underlying rather loose lamina propria (LP) contains Bowman's glands that extend ducts through the OE, fibroblasts, blood vessels, and nerve fascicles containing axons from OSNs in the OE (Nakashima et al. 1991; Morrison and Costanzo 1992). These fascicles cross the cribriform plate in order to synapse with secondary neurons in glomeruli of the OB (Richard, Taylor, and Greer 2010; Treloar et al. 2002). In contrast to laboratory rodent epithelium, prior studies on human biopsy and autopsy specimens reveal that the distribution of cells in human OE is less well ordered with wide variations in the neuronal abundance ranging from a robust neuroepithelium to a neuronally impoverished epithelium to aneuronal epithelium. In addition, patches of respiratory metaplasia are interspersed, i.e., what was olfactory epithelium has been replaced by an epithelium consisting of ciliated columnar epithelial cells and basal cells (Holbrook et al. 2011; Nakashima et al. 1991; Morrison and Costanzo 1992; Holbrook, Leopold, and Schwob 2005; Nakashima, Kimmelman and Snow, 1984).

Even though human as well as rodent OE is capable of lifelong regeneration thanks to the persistence of stem and progenitor cells within the basal cell population (Brann et al. 2015; Schwob 2002; Durante et al. 2020), a decline in smell function with age is well known in humans (Zhang and Wang 2017; Doty et al. 1984; Vennemann, Hummel, and Berger 2008; Lu et al. 2021). Deterioration in olfaction among the elderly likely depends to some degree on the extent of pathological alterations in the area, structure, and composition of the OE. Beside a general decrease of epithelial thickness, the OE from human and rodents loses mature olfactory sensory neurons (OSNs), undergoes reduction in vascularity and displays large areas of non-sensory respiratory epithelium (Paik et al. 1992; Naessen 1971; Attems, Walker, and Jellinger 2015; Mobley et al. 2014; Rosli, Breckenridge, and Smith 1999; Doty and Kamath 2014; Loo et al. 1996). Although not specifically known to be related to age, neuromas (abnormal patches of disorganized olfactory axons) and epithelial-lined submucosal cysts or "pits" are a commonly described alteration in human OE not seen to the same degree in laboratory rodents subject to normal aging (Holbrook et al. 2005; Trojanowski et al. 1991; Feng et al. 1997).

Compared to what is known for the OE, the literature on organization of the human OB is relatively sparse. Our current understanding of OB morphology is based mostly on rodents whereas the papers on human OB have shown dramatic differences between the two species. With reference to the organization of the glomerular layer, where OSNs and second order neurons synapse (Kauer and Cinelli 1993; Mori, Nagao, and Yoshihara, 1999) the number, size and shape of glomeruli is less regular in humans as compared to rodents with a high inter- and intraindividual variance (Maresh et al. 2008; Smith et al. 1991; Zapiec et al. 2017). Moreover, axons of incoming OSNs are observed extending deeper into the bulb than the typically ordered glomerular layer observed in rodents. Finally, individual periglomerular cell populations in the human bulb are not as easy to distinguish (Maresh et al. 2008; Smith et al. 1991; Zapiec et al. 2017).

Correspondingly little is known regarding any changes in OB histology with age in humans, although some might be expected given the intimacy of the connection between the periphery and the glomerular layer, and the potential correlation between age and the diminishment of the neuronal population of the OE. Decreases in bulb volume, glomeruli and frequency of synapses as well as atrophy in glomerular dendrites and mitral cells have been described as a function of age (Attems et al. 2015; Hang et al. 2015; Meisami et al. 1998; Hinds and McNelly 1981; Buschhüter et al. 2008). However, other studies have postulated stable glomerular density with increasing age (Richard et al. 2010; Mobley et al. 2014; Maresh et al. 2008). In general, due to difficulties in obtaining an adequate amount of autopsy specimen, studies on the human OB and OE are mostly limited to descriptive findings and detailed quantitative analyses are lacking.

Using a large sample of human autopsy specimens and analyzing both whole sheets of mucosa as well as histological sections, we performed an in-depth quantitative analysis on multiple parameters for the OE and OB identifying changes that relate to increasing age. Moreover, utilizing epithelium and bulb tissue originating from the same specimen we attempted to predict OB characteristics based on the condition of the olfactory periphery.

METHODS

Tissue acquisition and preparation

Post-mortem specimens including the OBs, cribriform plate, middle and superior turbinate, and septum spanning the distance from the frontal sinus to the sphenoid sinus were procured within 24 hours from time of death and fixed immediately by submersion in 10% formalin in water by the following collection centers: National Disease Research Interchange (NDRI, Philadelphia, PA), Advanced Bioscience Resources Inc. (ABR, Alameda, CA) and Anatomy Gifts Registry (AGR, Hanover, MD). Specimens arrived at our lab within 14–21 days. Information regarding age, gender, cause of death and comorbidities was provided for each specimen (Table 1). We had no information regarding olfactory function. Olfactory bulbs, olfactory epithelium and whole mucosal sheets were dissected and separated as described previously (Holbrook et al. 2011). In short, upon arrival the OBs were dissected from the cribriform plate and labeled to reflect orientation to position and side. The nasal cavity was then divided into the lateral wall and septal portions along the cribriform plate on each side. Whole mucosal sheets were removed from both the lateral wall and septum for whole mount staining analysis (Figure 1). A rectangular vertically oriented strip was removed from each whole mucosal sheet (Figure 1(c), (d)), oriented and embedded in optimal cutting temperature (OCT) compound (Miles Inc., Elkhart, IN), snap frozen, and then coronally sectioned at a thickness of 10–12μm using a cryostat (Leica CM3050S, Bannockburn, IL). OBs were also oriented, embedded in OCT, snap frozen in liquid nitrogen, and coronally sectioned at 10–16μm. Cut sections were mounted individually on Plus slides (Thermo Fisher Scientific, Pittsburg, PA) and stored at −20°C until staining.

Immunohistochemistry

The steps for immunohistochemistry were performed according to standard procedures in the laboratory (Holbrook et al. 2011). Frozen sections were thawed and rinsed in phosphate-

buffered saline (PBS) for five minutes to remove OCT. For permeabilizing and minimizing inherent peroxidase activity the slides were then treated with 0.1% H_2O_2 in PBS for 10 minutes. The sections were flooded with 0.01M citric buffer (pH 6.0) before placing the slides for 10 minutes in a common food steamer at 45°C for antigen retrieval. Slides were washed in PBS for five minutes and blocked 10 minutes in normal donkey block (NDB - 4% Bovine Serum Albumin (BSA), 5% Non-Fat Dry Milk (NFDM), 10% Donkey Serum, PBS, 0.1% Triton X-100). Primary antibodies were diluted in NDB, and the slides were incubated over night at 4°C in a humidified chamber. Primary antibodies that were used in this study and their staining conditions (concentrations and pretreatments), as well as the cell type recognized by each antibody, are listed in Table 2. Bound primary antibodies were visualized either by incubating with the corresponding biotinylated secondary antibody (Jackson ImmunoResearch Laboratories, Inc., West Grove, PA) followed by fluorescent streptavidin complexes or with a suitable fluorescently conjugated secondary antibody (Invitrogen, ThermoFisher Scientific, Waltham, MA). Tyramide signal amplification (TSA) was utilized to enhance T-box transcription factor (TBX21) and TH fluorescent signals according to kit instructions (PerkinElmer, Waltham, MA). Fluorescent sections were additionally submerged in DAPI or Hoechst to stain nuclei and then coverslipped with 0.1M n-propyl gallate. Staining specificity of the antibody used was either previously confirmed through antiserum incubation or confirmed with identical staining characteristics as previously reported elsewhere. Whole mount mucosa was stained in a similar fashion according to published procedure (Holbrook et al. 2011) using mouse anti-TUJ1 (1:2000) or rabbit anti-PGP9.5 (1:7,000) at longer incubation times than with sections. Peroxidase based staining was visualized using 3,3’-diaminobenzadine (DAB) as the chromogen. The stained whole mount mucosal sheets were flattened with weights on lysine coated glass slides and then dehydrated through increasing concentrations of ethanol. The slides were then cleared through xylene and coverslipped with DPX mounting media.

Image acquisition

Mosaic images of stained sections were taken on a Nikon Microphot-SA microscope (Nikon Instruments Inc., Melville, NY) with a 4x objective and driven with a Ludl motorized stage (Ludl Electronic Products Lid., Hawthorne, NY). Images were obtained with a Retiga camera (Teledyne QImaging, British Columbia, Canada) with iVision capturing software (BioVision Technologies, Exton, PA) and stitching software using Autopano Pro (Kolor, no longer supported). In some instances, stained sections were imaged on a Zeiss LSM800 confocal microscope. In all photos, only the balance, contrast, and evenness of illumination were adjusted. Image analysis and quantification were performed using ImageJ software (ImageJ 1.50i, https://imagej.nih.gov/ij/).

Whole mount analysis

Mosaic photographs of whole mount stained specimens were overlayed on images of the original tissue block taken post-mucosa removal. Distances from the stained area to anatomic landmarks of the nasal cavity were then measured. For purposes of centroid calculation, all specimen measurements were standardized to orient the posterior edge of the specimen to the left and anterior edge to the right; therefore, images from specimens not fitting this orientation were digitally flipped 180° along the horizontal axis. Shifts in the

distribution of olfactory neurons across the mucosal surfaces were assessed by comparing the centroid, or geometric center, of the olfactory area (areal centroid), which was delimited by a smooth outline encircling the stained neuronal elements, and the centroid of the object made up of the collective stained OSNs within this defined area (neuronal centroid). The neuronal centroid position (i.e., the geometric center of the distribution of stained neurons) was calculated using the following formula for the geometric decomposition method:

$$C_X = \sum \frac{C_{i_x} A_i}{\sum A_i}; C_Y = \sum \frac{C_{i_y} A_i}{\sum A_i}$$

where *Cix* and *Ciy* are the *x* and *y* coordinates for the centroid of each composite simple shape used to fill the object of interest and *Ai* is the area of each simple shape used. Any shifts in the position of the neuronal centroid from the geometric center was determined by subtracting the x and y coordinates of the areal centroid from the x and y coordinates of the neuronal centroid. The resulting difference in x and y coordinates were used to obtain a vector magnitude ($a^2 + b^2 = c^2$). The formula:

$$\theta = \tan^{-1}\left(\frac{Y}{X}\right)$$

was used to calculate the direction in shift of the neuronal centroid from the areal centroid relative to the x-axis of the tissue (oriented with the posterior edge to the left) with a value of zero aligning with the x-axis in the positive direction (anteriorly) and values ≥ 1° progressing counterclockwise around the areal centroid (origin of x and y-axis). In this manner and with this orientation, values from 0 to 90 and from 270 to 359 indicate a neuronal centroid shift anteriorly, and values from 90 to 270 indicate a neuronal centroid shift posteriorly. Similarly, values from 0 to 180 indicate a neuronal centroid shift dorsally and values from 180 to 359 indicate a neuronal centroid shift ventrally. Areas of denuded epithelium resulting from dissection and tissue processing as well as the region dissected for histologic analysis were removed from the overall object shape before calculating the centroids.

Tissue section analysis

Samples from 36 subjects (12 female) with an average age of 74.1 years (range 28–92) were used for analysis. A total of 15 subjects (5 female) included a medical history of dementia with 6 having a specific diagnosis (5 Alzheimer's, 1 Parkinson's Disease). Given variable autopsy conditions and tissue preservation, not all tissue from each subject could be used for all analyses. From 24 subjects a total of 39 bulbs (19 right, 20 left) were collected. Analysis of OBs and their matched corresponding OE were performed separately for right and left sides, if available. No samples were excluded. For OE analysis, epithelial sections from 29 subjects (27 septum, 18 lateral wall) were analyzed.

OE sections—Three evenly spaced sections of the OE encompassing the full dorsoventral axis of each mucosal strip were obtained from the right and left septum and/or right and left lateral wall, sampled, and averaged for each datapoint. When both septal and lateral

wall specimens were available from the right and left sides, the average value from the strips was used if the comparison of lateral wall vs. septum and right vs. left side did not reach significance by t-test and one-way ANOVA. Differences regarding age, dementia, and gender were assessed.

To assess the extent of neuronal maturation, β-tubulin III (TUJ1)-antibody positivity was used to identify and assess both mature and immature OSNs (Holbrook et al. 2011) and olfactory marker protein (OMP)-antibody positivity was used to identify and assess the population of mature OSNs (Monti-Graziadei et al. 1977). Total area of staining was calculated using ImageJ software and normalized to the measured length of OE ranging from the cribriform-plate edge dorsally to the border with continuous respiratory epithelium ventrally. A maturity index was calculated as a ratio of OMP(+) staining to TUJ1(+) staining in each OE section. In addition, TUJ1 staining was used to identify neuromas within the OE. Total length of the OE occupied by neuromas was also normalized to total OE length.

The overall condition of the tissue was determined in sections stained with antibodies to TUJ1 and to β-tubulin IV (BetaIV), which marks respiratory epithelium. Percent lengths of specific types of epithelia were calculated as follows: respiratory epithelium (BetaIV(+) staining), neurogenic/neuronal OE (TUJ1(+) staining), aneuronal OE (BetaIV(−)/TUJ1(−) staining) and mixed epithelium (BetaIV(+)/TUJ1(+) staining). In addition, sections labeled for BetaIV and TUJ1 were used to analyze the number and type of sub-epithelial cysts (TUJ1(+) neuronal cysts, BetaIV(+) respiratory cysts and TUJ1(+)/BetaIV(+) mixed cysts) within the lamina propria.

Sections adjacent to those stained for OMP/TUJ1 and BetaIV/TUJ1 were labeled with antibodies to KI67 and SOX2 to identify proliferating basal cells within the OE. Numbers of dividing basal cells from sections of right and/or left septum were averaged and normalized to OE length.

OB sections—Data obtained were collected separately for right and left olfactory bulbs. Measurement of OB length was defined as the distance between the first and last occurrence of glomeruli as identified by co-labeling with OMP and vesicular glutamate transporter type 2 (VGLUT2). To calculate bulbar volume, the surface area (SA) of 6 evenly spaced sections throughout the entire OB was measured using ImageJ software including the first and the last section. SA was then multiplied by distance between the sections to estimate total OB volume. The total expanse of positive VGLUT2 staining was quantified from five evenly spaced sections throughout the bulb by summating area of staining from each mosaic image measured with Photoshop (Adobe v12.0) and the threshold tool of ImageJ. Summed areas of glomerular staining were normalized to total OB surface area. OB mosaic images were divided equally into superior and inferior halves using ImageJ software and the amount of positive VGLUT2-staining was quantified for ventral and dorsal OB separately.

Statistical analysis

Statistical analysis and graph creation were performed using IBM SPSS Statistics (IBM SPSS Statistics ©; 23.0, for Mac) and SigmaPlot 12.0 (SYSTAT Software Inc.). For assessment of correlation between OE/OB measurements and age as well as between OE

and OB parameters a linear regression analysis was performed. Due to known effects of dementia on olfaction and the correlation of dementia with age, we tested for any contribution of a diagnosis of dementia to age-related differences in the composition of the specimens. In the case of a significant difference a multi-linear regression analysis was performed. Unpaired t-tests were used for comparing OE/OB parameters and dementia/gender; mean, standard error of the mean (±) and p-value (p) are displayed with each result. For those comparisons that didn't pass Levene's test for equality of variances, the Welch t-test was performed instead of a t-test. Due to the unilaterality of connections between OE and OB, left and right bulb originating from the same patient were treated as separate specimen, except when analyzing for correlation with age. For purposes of age correlation, OB parameters were averaged for right and left side. Before taking the average of two subgroups either a one-way ANOVA or t-test was performed to identify potential differences within the subgroups. If differences were found, subgroups were not averaged but analyzed separately.

In analysis of whole mount differences, a two-tailed t-test was used with normal value distribution (assessed with Shapiro-Wilk test), while a rank sum test (Mann-Whitney *U* test) was utilized when normality failed. For the comparison of epithelial measurements with age, a multi-linear regression analysis was performed setting dementia and age as independent factors. Figures were generated using PRISM software (GraphPad Prism ©; version 8.4.3 (471), for Mac) or Adobe Photoshop 2020 (22.0.0).

RESULTS

Whole mount analysis

Anatomical location of olfactory epithelium—To determine the location of OE in relation to known anatomic structures within the nasal cavity, the mucosae from the lateral nasal cavity and from the nasal septum were detached from the underlying bone and immunoperoxidase-stained for neurons as whole mounts (Figure 1(c), (d)) and then were matched to the resected margins (Figure 1(a), (b)) from the original tissue block. Distances from the stained margin of OE to known anatomic landmarks were then measured (Figure 2). Measurements were noted to vary across specimens. However, on average, the boundary of olfactory epithelium on the lateral nasal cavity extends 1.0 cm below the cribriform plate, 0.7 cm posterior to the anterior attachment of the middle turbinate, 1.7 cm above the inferior edge of the middle turbinate, and 0.4 cm anterior to the sphenoid face. The septal OE location mostly mirrors the lateral boundaries. Stained olfactory neurons were never observed at the anterior edge of the middle turbinate in contrast to previous reports (Leopold et al. 2000). Remarkably the area of OE in relation to anatomic structures of the nasal cavity was very similar in adults to embryonic samples (Figure 3) and just smaller in scale.

Olfactory neuronal area as a function of age and dementia—We compared whole mount staining of OE in embryonic specimens with adult specimens and observed two major differences (Figure 3(a), (b), (c)). In embryonic tissue, the margins of the OE are smooth and well demarcated from the respiratory epithelium (RE) as opposed to the erratic edges of adult OE. As with adult olfactory area, the embryonic OE is located under the cribriform

plate with the anterior margin posterior to the middle turbinate attachment and mostly confined to the area of the superior turbinate (Figure 3(a)). Embryonic OE is composed of a densely stained, continuous sheet of olfactory neurons, while adult OE is commonly interrupted by areas in which OSNs are completely absent. As previously identified, and further characterized below, the interspersed aneuronal epithelium within the confines of the olfactory area consists of neurogenically exhausted OE which is recognizable in sections by the presence of microvillar-capped Sus cells, or metaplastic RE, which contains ciliated, columnar, respiratory-like epithelial cells.

The olfactory area as a whole – defined as the region encompassed by the border of olfactory epithelium with the contiguous sheet of respiratory epithelium and including both neuronal and aneuronal regions – varies between specimens but is consistent between the right and left nasal cavities with a larger area ($p = 0.043$) on the lateral side (1.724 cm^2) compared to the septum (1.366 cm^2). Given the changes noted in adult tissue compared to embryonic specimens, we tested for an effect of age on the size of the olfactory area. Due to known effects of dementia on olfaction and the correlation of dementia with age, the presence of dementia was included in the analysis. Consequently, we performed a multi-linear regression analysis of OE area across specimens averaging the right and left sides when both samples were available from the cadaver block. When all specimens were analyzed, independent of dementia diagnosis, OE area decreases significantly with increasing age in the septal specimens (Figure 3(d)); when specimens with a known diagnosis of dementia are separated for analysis, no significant relationship was identified ($p = 0.722$, septum; $p = 0.142$, lateral). The regression lines were weaker for lateral wall specimens and did not reach significance.

To assess the diminution of neuron-containing OE within the olfactory area as a function of age, we calculated the percent of the olfactory area that contained neurons immunopositive with PGP9.5 or TUJ1 antibodies, which we term % remaining OE. Again, there was no difference between the right and left nasal cavities, nor was there any significant difference between the average % remaining OE on the septum (72.9%) and lateral nasal wall (71.3%; $p = 0.66$). Using multilinear regression, we find a statistically significant effect of increasing age on decreasing % remaining OE for both the septum and lateral wall (Figure 3(e)). When specimens from dementia subjects are analyzed, the same effect of age on reduction of % remaining OE is seen in nasal septum specimens ($p < 0.001$) but is not significant for the lateral wall ($p = 0.071$).

Olfactory neuron density shift with age—As mentioned above, the specimens from embryonic tissue revealed continuous sheets of OE without interspersed regions of aneuronal OE or metaplastic RE. Given the loss of OE with age in the specimens presented here and the shift in overall distribution of neurons in the OE of aged rodents posterodorsally (Loo et al. 1996), we predicted that the loss of neuron-containing OE is worse in anterior and inferior regions of the olfactory area where higher airflow and greater environmental exposure is likely to occur (Keyhani, Scherer, and Mozell 1997). To assay for a geographic shift in the distribution of OE with age, we determined the geometric center, or centroid, of the olfactory area (areal centroid as defined in methods) and compared it with the centroid of the shape that encompasses the retained neuron-containing OE within that area

(neuronal centroid; Figure 4(a)). We observed an average centroid shift across all adult septal specimens of 2.14 mm (SEM ± 0.30 mm) with an average direction of 146.14° ± 11.66° (SEM) with the sample oriented with posterior to the left, 0° pointing anteriorly, and increasing angle progressing counter-clockwise; thus, the centroid of the neuronal composition of the OE area is displaced to a more posterior and dorsal position (i.e. more neuronal dense) as compared to the centroid of the olfactory area, as predicted. The average centroid shift in lateral specimens was 2.11 mm ± 0.20 mm (SEM) with an average direction of 151.19° ± 14.28° (SEM) and not significantly different from the septum values ($p = 0.388$ and $p = 0.919$; respectively). We also tested for changes in centroid shift as a function of age and dementia and combined the septum values with the lateral wall values given the lack of differences between the sides. Although there appears to be a trend toward increasing centroid shift direction and magnitude with age, the contributions of age and dementia lacked significance (Figure 4(b), (c)).

Analysis of olfactory epithelium section

Immunohistochemical characterization of human OE sections—To provide a histologic basis for what would be considered healthy adult human OE and to determine suitable parameters for a quantitative analysis, sections from adult human OE were stained using antibodies directed against cell-specific markers and transcription factors and compared to fetal OE (Figure 5). Our observations are largely consistent with findings described in previous published articles (Holbrook et al. 2011; Nakashima et al. 1984, 1991; Morrison and Costanzo 1992; Holbrook et al. 2005). Overall, the entirety of the fetal epithelial sample and regions of healthy adult human OE resemble that described in rodents. OE is identified by its characteristic pseudostratified columnar epithelium composed of mature and immature olfactory neurons labeled using β-tubulin III (TUJ1) in the middle zone of the epithelium, microvillar-capped sustentacular cells that populate the apical surface, basal cells, and Bowman's glands/ducts. In the embryonic OE, the zone occupied by the population of olfactory neurons is slightly thicker as compared to the thickest and healthiest-appearing adult tissue (Figure 5(a), (b)). Metaplastic respiratory epithelium (RE), which is identified by surface staining with antibodies against β-tubulin IV (BetaIV), is absent from regions of healthy adult OE and non-existent in embryonic OE (Figure 5(b)), however regions of metaplastic RE and areas of aneuronal OE are frequently found in adult samples (see Figure 7) as described previously (Holbrook et al. 2005; Paik et al., 1992; Nakashima et al., 1984, Child et al., 2018). Multiple layers of neurons at various stages of maturation comprise the central zone of typical healthy OE, however, OMP(+) mature olfactory neurons are found to be less strictly limited to the more apical aspect of the neuronal layer in humans as compared with rodents (Figure 5(a)). The horizontal basal cells (HBCs), globose basal cells (GBCs), and supporting cells are labeled with antibodies directed against the transcription factor, SOX2 (Figure 5(c)). Adult HBCs can be identified in a single row along the basal lamina and are typically mitotically quiescent and unlabeled by antibodies to the cell cycle marker KI67. SOX2(+) GBCs that are situated apical to the HBCs are distributed in clusters and are frequently double-labeled with KI67 and actively proliferate (arrows, Figure 5(c)). Fetal OE differs from the adult composition in several respects. HBCs are recognized by expression of p63 as in adult OE but are disposed as a more discontinuous basal monolayer in embryonic tissue (Figure 5(d)), which is consistent

with presence of a more uniform layer in adult rodents as well (Holbrook, Szumowski, and Schwob 1995; Packard et al. 2011). GBCs appear reduced in number and are also not uniformly distributed in the tangential plane of the epithelium (Figure 5). A palisade of supporting cell nuclei labeled with SOX2 is seen at the apical level of the epithelium in both adult and fetal OE (dotted rectangle, Figure 5(c)). Bowman's gland and duct cells are identified using an antibody against SOX9. As expected, SOX9(+) Bowman's gland cells are located within the lamina propria (LP) (dotted circle, Figure 5(d)) with occasional duct cells extending into the epithelium in both adult and fetal tissue (arrows, Figure 5(d)).

Neuronal status as a function of age and dementia within OE—We obtained usable tissue sections of OE from 29 individuals for immunohistochemical analysis of the epithelium (average total analyzed mucosal length = 5.8mm ± 0.36 mm (SEM)). We analyzed the neuronal composition of OE vertical strips by quantifying total TUJ1(+) OSNs staining and total OMP(+) mature OSNs staining as a function of OE length. An OSN maturity index (total OMP(+) staining/total TUJ1(+) staining) across mucosal strips was calculated from the septum (n = 27) and lateral wall (n = 18). Linear regression of septal mucosal specimens demonstrated no statistically significant differences in mature OSN staining, total OSN staining, nor the maturity index as a function of age (Figure 6(a)). However, analysis of lateral mucosal specimens revealed a significant decrease of both mature OSN ($p = 0.002$, $r^2 = 0.47$) and total OSN ($p = 0.015$, $r^2 = 0.32$) staining as a function of increasing age. No significant age-related correlation was observed for the OSN maturity index ($p = 0.12$, $r^2 = 0.14$) which suggests that any decrease in number of OSNs we found with age is not associated with a disproportionate loss of neuronal maturity from lack of olfactory bulb targeting and trophic support. After averaging values from septal and lateral mucosal strips, only the amount of mature OSN staining ($p = 0.02$, $r^2 = 0.18$) revealed a significant inverse correlation with advancing age. There were no significant differences for either of the described three parameters with respect to dementia regardless of whether values originated from septal or lateral mucosal strips (Figure 6(b)).

Regeneration activity related to age and dementia—The OE is known to respond to insults or neuronal loss with increased basal cell mitosis and regeneration of epithelial cell components, however this capability is known to decrease with age in some animal models of aging and is likely to be characteristic of human aging given the reduction in neurogenic OE (Holbrook et al. 2005; Nakashima et al. 1984, Child et al. 2018). We estimated regenerative activity of OE basal cells by counting basally positioned KI67(+)/SOX2(+) dividing cells in septal mucosal strips (n = 27; average number of total KI67+/SOX2+ basal cells = 14 ± 2.08 (SEM)) and assayed for the effect of age. Although using KI67(+)/SOX2(+) labeling to identify OE basal cells ignores the complete repertoire of mitotically active and inactive GBCs involved in OSN regeneration, it does capture dividing basal cells that would expect to increase as a result of neuronal depletion. Instead, we found a decrease in the number of dividing basal cells with age that would suggest either decreasing overall numbers of OE basal cells or decreased regenerative activity, however the result did not reach significance ($p = 0.059$, $r^2 = 0.14$) (Figure 6(c)). The number of dividing basal cells did not differ significantly with respect to dementia (data not shown).

Extent of epithelial metaplasia related to age and dementia—As mentioned above, in humans it is common to observe relatively healthy, neuron-containing OE adjacent to metaplastic regions of respiratory epithelium (RE), aneuronal/neurogenically exhausted epithelium, or mixed features (Figure 7(a), (b)); a finding also typical of rodent models of aging (Child et al. 2018; Håglin, Berghard, and Bohm 2020; Kondo et al. 2009). To quantify the extent of the pathological deterioration in the OE, sections obtained from the excised strips of mucosa were stained with anti-BetaIV-tubulin and TUJ1. The lengths of epithelium with BetaIV staining (respiratory), TUJ1 staining (neuronal), mixed Beta-IV and TUJ1staining (mixed epithelium) and absent staining with either antibody (aneuronal) were measured from septal specimens (n = 27) and calculated as a percent total length of the distance from the dorsal margin of the tissue to the ventral most boundary of OE with continuous RE. We found a significant increase of mixed epithelium with age (Figure 7(a); $p = 0.01$, $r^2 = 0.22$). However, no significant difference in percent of RE or aneuronal OE was observed as a function of age. As with measurements for evaluation of the neuronal status there is no significant correlation observed for any of the described parameters with respect to dementia (not shown).

Presence of submucosal epithelial cysts—Within the adult OE, submucosal cysts lined by a true epithelium are commonly observed as described previously (Nakashima et al. 1991; Feng et al. 1997). Some cysts appear to be enlarged Bowman's gland lumens. However, additional non-glandular cystic structures can be categorized on the basis of labeling with anti-BetaIV or TUJ1 into TUJ1(+) neuronal, BetaIV(+) respiratory, or BetaIV(+)/TUJ1(+) mixed cysts (Figure 7(b), (c)). The cysts show wide variations in size and shape and are occasionally seen erupting through the epithelial surface (Figure 7(c)). In many cases the epithelium overlying large cysts is thinner and metaplastic with RE or aneuronal characteristics. In regions where the cysts open into the epithelium, they appear to merge continuously with the epithelium of the same area. Interestingly, cysts were absent from fetal tissue samples suggesting that they form as a response to injury, stress, or aging. We counted respiratory, neuronal and mixed cysts along strips of septal mucosa (n = 27). No age or dementia-related differences were observed (not shown). However, we tested the correlations between total number of cysts and the extent of aneuronal OE and metaplastic RE (Figure 7(d)) and identified a significant correlation between the total number of cysts and the extent of respiratory metaplasia (percentage RE − $p = 0.005$, $r^2 = 0.27$) and the extent of neurogenic exhaustion (percentage aneuronal OE; $p = 0.02$, $r^2 = 0.2$). An expected decreased number of cysts occurred with larger regions of neurogenic OE. The degree of correlation between number of neuronal cysts and extent of neuronal epithelium, or respiratory cysts and extent of metaplastic RE was not statistically significant (not shown).

Epithelial neuromas—Neuromas were prevalent within human OE specimens as has been described previously with biopsies (Holbrook et al. 2005; Trojanowski et al. 1991; Holbrook, Rebeiz, and Schwob 2016). The size of the neuromata varied greatly among specimens, and typically stain densely for the neuronal marker TUJ1 but lack DAPI stained nuclei and OMP labeling (Figure 8(a)). As with epithelial cysts, we failed to identify neuromas in fetal OE, and the presence has been suggested to reflect previous damage to the adult OE (Holbrook et al. 2005; Schwob, Youngentob, and Meiri 1994). For purposes

of quantification, the total length of OE strips occupied by neuromata was measured as a percent length for septal (n = 27) and lateral (n = 18) mucosal samples and the average of both mucosal strips (n = 29). We found that the percent length of OE occupied by neuromata increases with advancing age in septal mucosal samples but does not reach statistical significance ($p = 0.06$, $r^2 = 0.13$). The trend toward significance was also observed when the values for septal and lateral mucosal strips were averaged ($p = 0.05$, $r^2 = 0.13$) but a correlation was not apparent in lateral specimens (Figure 8(b)). Of the adult specimens, neuromas were absent from samples obtained from individuals younger than or equal to 60 years of age. In addition, no correlation was found between total neuroma length and dementia (not shown).

Analysis of human olfactory bulb

Immunohistochemical characterization of human OB—Only a very few papers have described the human olfactory bulb (OB) with detail. We used OMP staining to mark the mature olfactory axons as they projected into the bulb and vesicular glutamate transporter type 2 (VGLUT2) staining to identify the synapses that the olfactory axons form within the neuropil of the glomerular layer (Figure 9(a); Maresh et al. 2008). There were notable differences in the microstructure of the bulb by comparison with rodents and other non-primates. The olfactory nerve layer in the adult bulb is relatively thinner as compared to the bulb from fetal specimens. Unlike the more regular single-layer of roughly spherical glomeruli that is typical of the rodent OB, the glomeruli in the human adult bulb are less orderly, are often disposed in multiple layers, and tend to extend more deeply into the bulb, which mirrors previous descriptions (Maresh et al. 2008; Zapiec et al. 2017). Broadly speaking, the distribution, size, and shapes of adult human glomeruli mirrors the disordered appearance and variations of shape and size that are typical of the rodent OB during recovery from injury, particularly the reinnervation observed after long-standing, but partially reversible denervation (Child et al. 2018; Cummings et al. 2000; Holbrook et al. 2014). Glomeruli of fetal OBs differ from adults having the appearance of budlike structures that are smaller in size and are arranged in a singular layer.

Sections stained with anti-tyrosine hydroxylase (TH), which identify dopaminergic periglomerular cells, can be found in embryonic and adult OB surrounding individual glomeruli (Figure 9(b)). In contrast to adult, TH(+) periglomerular somata in the embryonic OB appear tightly apposed to the glomerular layer and frequently congregate in areas with less glomeruli. Mitral and tufted cells of the OB can be visualized using antibodies to the T-box transcription factor TBX21 (Faedo et al. 2002). In our samples, the mitral cells in adult OBs are found singularly and intermittently over the external plexiform layer opposed to the formation of a coherent uniform layer deep to the glomerular layer seen in fetal OB (Figure 9(c)).

OB dimension related to age and dementia—Intact OBs that remained attached to the cribriform plate were obtained from 24 (23 for analysis of glomeruli) autopsy specimens. A total of 39 (35 for analysis of glomeruli) OBs were analyzed with respect to the OMP(+) axonal processes of the OSNs and their VGLUT2(+) synapses with second order neurons within the glomerular neuropil (Child et al. 2018; Gabellec et al. 2007). Bulb

length was calculated from the number of sections between the first and last recognized VGLUT2-stained glomeruli and averaged 10.85 ± 0.32 mm (SEM), ranging from 6.59 to 15.54 mm (n = 39). Bulb volume was calculated from the area of individual sections sampled systematically through the length of the OB, with known section thickness, and known number of intervening sections. We calculated an average bulb volume of 51.24 ± 2.04 mm^3 (SEM), with a range of 25.68 to 94.89 mm^3 (n = 39). In specimens from individuals aged 70 or older, mean OB volume was 47.83 ± 1.47 mm^3 (SEM) and ranged from 25.68 to 62.65 mm^3. As a function of increasing age, total bulb volume decreases significantly ($p = 0.02$, $r^2 = 0.25$). Results roughly correspond with previous MRI-based age-related normative data of OB volumes from 125 subjects without olfactory dysfunction (Buschhüter et al, 2008). The data indicate that people older than 45 years have a minimum bulb volume of 46 mm^3. Slightly higher bulb volumes measured in our study could be due to high interindividual variances in bulb volume (Buschhüter et al. 2008) and differences in the approach technique (MRI vs. autopsy material). Dementia was not found to correlate with OB volume.

Glomerular distribution—Given the difficulty in recognizing discrete glomeruli in adult OB sections, instead of attempting to count individual glomeruli we measured the cumulative area occupied by VGLUT2(+)-staining normalized to the total OB area as a representative measurement of overall glomerular volume in 35 bulbs from 23 specimens. The relative area of the glomerular neuropil calculated in this manner was 1.65 ± 0.17 % (SEM) and ranged from 0.6 to 3.49 %. We anticipated that a relatively greater extent of olfactory axonal innervation of the bulb would correlate with higher total bulb volume. Indeed, we found a positive correlation between relative VGLUT2(+)-staining and increased bulb volume ($p = 0.05$, $r^2 = 0.11$). We also observed variability in density of innervation based on topography, such that the ventral surface of the bulb adjacent to the cribriform plate was more heavily innervated than the dorsal half (1.04 ± 0.1 % (SEM) vs. 0.47 ± 0.08 % (SEM), respectively; $t = 3.95$, $p = 0.0003$, unpaired t-test) (Figure 10(a)). Given the reduction of mature OSNs as a function of age, we tested whether VGLUT2 stained glomeruli also decreased with increasing age and found staining decreases significantly ($p = 0.002$, $r^2 = 0.38$) (Figure 10(b)). When the effect of age on innervation to dorsal bulb is compared with that to the ventral bulb, innervation is significantly diminished with age in the ventral half ($p = 0.006$, $r^2 = 0.31$) but has no correlation in the dorsal half ($p = 0.44$, $r^2 = 0.03$). No other gender or dementia related differences in VGLUT2 staining were observed.

Intra-subject correlations between OE and OB

To determine whether the neuronal status of the olfactory periphery directly predicts and potentially impacts the glomerular status of the OB on an individual basis, we tested for correlations between various OE and OB parameters between samples of epithelium and bulb obtained from the same autopsy subject. No significant correlation was found between the relative glomerular area of the OB and mature and total OSN staining or OSN maturity index in the OE within the same autopsy subject. Given the significant correlation between ventral glomerular area and age, we compared neuronal status in the OE and the amount of VGLUT2 staining in the ventral bulb and found a positive intra-individual correlation

between ventral glomerular VGLUT2 staining and mature OSNs ($p = 0.02$, $r^2 = 0.24$, $n = 21$). No other measure of epithelial status was correlated with glomerular innervation.

DISCUSSION

We present a unique, broad-based analysis of the human peripheral olfactory system and its neuronal projection onto the olfactory bulb as a function of age utilizing a macroscopic and microscopic examination of autopsy specimens. Immunohistochemical staining of whole mucosa sheets allows for a global, broad-view assessment of changes in the olfactory periphery. Further in-depth observations from stained sections obtained from mucosal strips and olfactory bulbs demonstrate a general reduction in the olfactory neuronal population with age, while on an individual level, the neuronal density within the epithelium predicts the degree of glomerular synapses within the bulbs.

We looked at fetal olfactory tissue as pristine examples to compare with changes that may occur over time with adult tissue. The OE location in the embryonic nasal cavity is similar to what we find in the adult relative to other nasal structures. It displays a continuous, uninterrupted sheet of neuronal epithelium with smooth well-demarcated boarders adjacent to respiratory epithelium. This is in contrast to adult tissue where a deterioration of the system occurs with age, and the OE becomes patchy with erratic boarders, increasingly interrupted with areas of aneuronal and respiratory epithelium (Holbrook et al. 2011; Holbrook et al. 2005; Paik et al. 1992; Witt et al. 2009) similar to observations in mouse models of olfactory aging (Child et al. 2018; Håglin et al. 2020; Kondo et al. 2009). Although a consistent regenerative capacity of the vomeronasal organ and OE of rodents even during advanced stages of age including ability to respond to acute demands from chemical or surgical lesioning has been demonstrated (Brann and Firestein, 2010, Brann et al. 2015), the artificial housing environment of laboratory animals devoid of toxins and viral insults likely reduces chronic stress on the basal cells that could contribute to their exhaustion over time. Omura and colleagues recently showed a decrease in mature olfactory axons in superior turbinate and apposing septal mucosa from a dorsal to ventral position among all samples (Omura et al. 2021). Human biopsy studies have also suggested greater representation of olfactory neurons in posterior-dorsal regions of the nasal cavity (Feron et al., 1998). We find additional deterioration of neuronal rich OE progressing from an anterior-ventral to posterior-dorsal direction with a skew of higher density neurons in the posterior and dorsal regions of the nasal cavity that is more pronounced with older age. This may relate to the vulnerable position of anterior and ventrally located neurons in the nasal cavity that are more subject to air flow and exposure to insults such as environmental toxins or viral infections which are known to damage the OE, provoke different types of cellular destruction (Douek, Bannister, and Dodson 1975), and contribute to clinical olfactory dysfunction since number of mature OSNs is directly related to olfactory function (Hummel et al. 2017; Ajmani et al. 2016; Mori and Sakano 2011). Despite the reduction in mature OSNs no increased cell death or compensatory cell proliferation is evident in these areas (Omura et al. 2021). Common occurrence of observed respiratory metaplasia seen in adult tissue may arise as a default protective epithelium after neurogenic exhaustion (Child et al. 2018) and can be seen with severe direct damage due to the herbicide 2,6-dichlorobenzonitrile (DCBN) (Xie et al. 2013).

Our quantitative assessment of neuron-containing OE as well as amount of mature OSNs in OE from sections of olfactory mucosal strips reveal a significant inverse correlation with advancing age that supports our whole mount observations. However, even in the most advanced ages, our autopsy specimens contain some amount of OSNs in the olfactory mucosa despite the known clinical anosmia that commonly occurs in the elderly population (Doty et al. 1984; Hummel et al. 2007). This would suggest a critical mass of innervating OSNs may be required to allow for useful olfactory perception. However, a central etiology that would be reflected in an observed peripheral neuronal loss may provide an equal alternative explanation.

Besides the diminution of neuron-containing OE, the adult epithelium evinced neurogenic exhaustion, respiratory metaplasia, submucosal cysts and neuromata, which contrasts with the uninterrupted sheet of olfactory neurons present prior to birth. As mentioned above in adult humans, it is common to observe areas of relatively healthy neuron-containing OE adjacent to metaplastic regions of respiratory epithelium and/or neurogenically exhausted epithelium. Despite our data showing diminished olfactory neurons as a function of age, we did not find an expected significant age-related increase in respiratory metaplasia. This could be explained by our working definition of the olfactory area as the region between the cribriform plate dorsally and the ventral boundary demarcated by the last olfactory neurons encountered before the contiguous RE ventrally. As noted with our whole mount centroid analysis, there is a reduction in OE area with a shift of neuronal density toward the dorsal and posterior regions with age. Therefore, it is highly probable that a considerable portion of ventral mucosa beyond the last olfactory neuron was once neuronal and olfactory but transitioned to respiratory over time (Paik et al. 1992; Nakashima et al. 1984; Féron et al. 1998). The inability to differentiate metaplastic RE from original RE at the margins of the olfactory mucosa would result in an underestimation of the total amount of respiratory metaplasia. As further evidence for this unrecognized increase in respiratory metaplasia, we did find an increase in mixed areas of RE/OE with age, which likely represents a transitional stage before olfactory epithelium turns completely respiratory. Regardless, in humans, there appears to be a lack of an accelerated GBC response to neuronal loss which typically act to replenish the requisite neuronal population and preserve olfactory function. The regenerative capability is known to decrease with age in animal models of aging and is likely to be characteristic of human aging given the emergence and expansion of aneurogenic OE (Holbrook et al. 2005; Nakashima et al. 1984; Child et al. 2018). We found the dividing basal cell GBC population trends towards decreasing numbers with advancing age. Although our results were not statistically significant, we chose KI67+/SOX2+ labeling as our representative marker of dividing basal cells. The frequency of counted positive cells with this method was relatively low, and a more complete analysis of the GBC population may have provided larger cell counts to detect significance. A decrease in basal cell numbers or activity as a cause for diminished neurons is also supported by our finding of unchanged maturity index with increased age. For example, we would have expected a higher number of immature neurons compared to mature (lower maturity index) if a decrease in end-target trophic support was considered as a mechanism of age related neuronal loss. As shown in animal experiments utilizing direct epithelial injury and our accelerated turnover model of olfactory aging, OE is reestablished only in areas where multipotent global basal cells

are preserved, whereas areas absent of GBCs are repopulated with metaplastic respiratory epithelium (Jang, Youngentob, and Schwob 2003; Child et al. 2018). In experimental animals, areas of aneuronal and metaplastic RE devoid of GBCs retain dormant horizontal basal cells (HBC). Similarly, we find extant HBCs throughout our autopsy specimens regardless of respiratory metaplasia or aneuronal changes suggesting absent signaling of HBC activation with limited regenerative capacity during the natural aging process. Recent published data has implicated induction of inflammatory pathways as a possible mechanism for decreased OE stem cell function. Normal olfactory neuron activity and epithelial renewal appear to be vulnerable to inflammatory influences as stem cells functionally switch from regeneration to immune defense roles (Chen et al., 2019). In addition, olfactory stem cells from patients with age-related smell loss show inflammatory-response related molecular changes that appear to impair stem cell activation and epithelial homeostasis (Oliva et al., 2022). We recognize that an analysis of inflammatory mediators or inflammatory cells in our samples could have added further information to this potential mechanism of limited OE stem cell activity in advancing age.

We found no age-related correlation with number of submucosal cysts in our samples, yet they occur commonly within adult olfactory mucosa and were not observed in fetal tissue. Respiratory metaplasia was often found co-localized over submucosal cysts in many of our samples, and in some cases eruption of submucosal respiratory cysts were observed contributing to a patch of respiratory metaplasia. Such colocalization of cysts and metaplastic epithelium has been previously described in a mouse model of aging (Kondo et al. 2009). We found the total number of cysts to be correlated with the amount of neuronal impoverished epithelium suggesting they may play a role in the degeneration of the surface epithelium or alternatively occur in response to degeneration with an attempt to regenerate damaged OE (Nakashima et al. 1991). However, neither the correlation between the number of neuronal cysts and the reduction in neuronal epithelium nor between respiratory cysts and extent of metaplastic RE were statistically significant.

A loss of OSNs in the olfactory periphery reduces sensory innervation of the OB (Child et al. 2018). Therefore, a similar loss of glomeruli with age and a reduction in OBV would be predicted based on our findings in OE. Indeed, we observed a decrease in OBV and VGLUT2 staining as a function of age. OB volume correlates with olfactory performance independent of confounding factors such as gender, nasal congestion and smoking status (Lu et al. 2021). Accordingly, decreasing bulb volume with age may represent a histopathological correlate for age-related smell loss. Contrary to our result of decreasing VGLUT2 staining with age other studies postulate a stable glomerular density with increasing age (Maresh et al. 2008; Richard et al. 2010; Mobley et al. 2014). The divergence of our results from published data (Maresh et al. 2008) may reflect: differences in 1) the sample size; (Maresh et al. 2008) analyzed 7 samples as compared to 39 from (23 subjects) in our study, 2) the analytic approach; (Maresh et al 2008) separated their subjects into two subgroups (over 50 years and under 50 years) and performed an unpaired t-test, whereas we chose the linear regression model to look for a correlation between age and amount of glomeruli, and 3) the measurement approach; while (Maresh et al. 2008) manually counted individual glomeruli, we found it difficult to identify and count distinct

glomeruli and instead used the overall VGLUT2 staining to better identify glomerular synapses.

The ventral surface was more heavily innervated than the dorsal half possibly due to its position directly adjacent to the cribriform plate, and innervation was significantly diminished as a function of age only in the ventral half. Moreover, our analysis on a direct correlation between OE and OB reveal that the amount of ventral glomerular staining is directly correlated with the amount of mature OSNs in the corresponding OE. As established in rodents, the axons of OSNs from specific regions of the nasal cavity in humans may also target to glomeruli in specific regions of the olfactory bulb. Perhaps the dorsal OB innervation in humans derive from OSNs that are within more protected areas of dorsal OE. In return, the ventral OB regions could be innervated by a majority of anteriorly and ventrally positioned OSNs in the nasal cavity that are more vulnerable to injury resulting in loss of ventral synapses within the OB over time.

Other differences between aged and embryonic OBs were seen. Ectopic/invasive glomeruli that extended into deeper regions of the bulb past the typical glomerular layer were commonly found in adult human OB. Ectopic glomeruli are thought to be a result of aberrant connections of OSN with deeper layers of the OB (Hoogland, Berg, and Huisman 2003). The mitral cell layer that was compact in embryonic OB was indistinct in aged OB. Consistent with published findings (Smith et al. 1991; Bhatnagar et al. 1987), we found mitral cells in adult OB reduced in number and scattered over the external plexiform layer in a diffuse fashion. The disorganization of the mitral cells may remove a chemical/physical barrier (Treloar et al. 2002) that would prevent OSNs from penetrating into deeper regions of the bulb given that olfactory axons can invade neuropil in other parts of the central nervous system when deprived of their normal target (Graziadei and Samanen 1980). Given that abnormal glomerular structure and ectopic glomeruli appear after damage to the OB (Hoogland et al. 2003), the accumulation of these structures may indicate epithelial attempts at recovery, the functional consequence of which is unknown.

Several technical aspects and limitations of analyzing whole mucosal sheets and mucosal strips need additional consideration. Statements on histomorphology in human OE based on the analysis of mucosal strips are restricted to a limited area of the OE and extrapolation to the entire olfactory mucosa has to be taken cautiously. To provide a better global assessment of the periphery, analysis of whole mucosa sheets was performed. However, complete whole mount staining of the entire olfactory mucosal sheet is a more difficult process. Whole mount staining cannot be repeated if failed on the first attempt leading to an overall lower number of specimens for complete analysis. Additionally, some of the acquired specimens did not arrive with complete and intact olfactory mucosa requiring their exclusion from various analyses. During tissue acquisition and processing, mucosal areas can become abraded with loss of epithelium. By necessity, these areas were removed from analysis of neuronal density. In these cases, an assumption is made that neuronal density is the same as the surrounding intact epithelium, and the removal from analysis would not significantly impact the overall results. However, this assumption would underestimate gradients in neuronal density, and therefore our whole mount results likely reflect a true change with age.

Regardless of technical issues, inherent difficulties in assessing OE health derive from the findings that respiratory metaplasia and olfactory degeneration are also present in normosmic adult patients (Holbrook et al. 2005; Paik et al. 1992; Witt et al. 2009; Naessen 1971) making the correlation of olfactory epithelial pathology with olfactory dysfunction difficult. Unfortunately, data regarding olfactory ability, dysfunction or information specific to history of nasal/sinus inflammation in our samples was not available making direct correlation with olfactory ability impossible. Instead, we rely on the established known correlation of age with human functional olfactory loss based on published psychophysical testing data (Doty et al. 1984; Hummel et al. 2007). Our samples are also weighted towards more advanced adult ages given the increased availability of autopsy specimens from elderly populations, and the data from the youngest specimen substantially contributed to significance in our statistical analysis in many cases. However, considering the lack of findings associated with age in the fetal tissue and the milder degree of these findings in the young adult, we believe the data from this specimen is important to the analysis as a whole and shouldn't be considered an outlier. To be able to make a stronger statistical statement regarding age-related differences a larger sample size of young specimens would be ideal in future studies. Lastly, our analysis of changes with onset of dementia also relied on the limited information provided with the autopsy specimens. Under-reporting of dementia most certainly would contribute to the lack of correlation with histology.

In sum, the present study provides an in-depth assessment of anatomical changes in adult human olfactory tissue and reveals insights into histomorphologic correlates for age-related smell loss. We observe a general decrease in olfactory neurons as a function of age, which is reflected in a reduction in glomerular synapses. The findings of metaplastic respiratory regions and neurogenically exhausted epithelium with concomitant trend in the reduction ofdividing basal cells suggests the emergence of stem cell quiescence as an underlying mechanism for age-related smell loss and a possible target for future therapeutic intervention.

ACKNOWLEDGMENT:

We thank Po Kwok-Tse for her technical assistance and Jacob Hangen for additional histologic procedures.

FUNDING:

This work was supported by NIH R01 DC010242

DATA AVAILABILITY STATEMENT:

The datasets generated during and/or analyzed during the current study are available from the corresponding author on reasonable request.

REFERENCES

Ajmani Gaurav S., Suh Helen H., Wroblewski Kristen E., Kern David W., Schumm L. Philip, McClintock Martha K., Yanosky Jeff D., and Pinto Jayant M.. 2016. "Fine Particulate Matter Exposure and Olfactory Dysfunction among Urban-Dwelling Older US Adults." Environmental Research 151:797–803. doi: 10.1016/j.envres.2016.09.012. [PubMed: 27692900]

Attems Johannes, Walker Lauren, and Jellinger Kurt A.. 2015. “Olfaction and Aging: A Mini-Review.” Gerontology 61(6):485–90. doi: 10.1159/000381619. [PubMed: 25968962]

Bhatnagar Kunwar P., Kennedy Ray C., Baron Georg, and Greenberg Richard A.. 1987. “Number of Mitral Cells and the Bulb Volume in the Aging Human Olfactory Bulb: A Quantitative Morphological Study.” The Anatomical Record 218(1):73–87. doi: 10.1002/ar.1092180112. [PubMed: 3605663]

Brann JH, and Firestein S (2010). Regeneration of New Neurons Is Preserved in Aged Vomeronasal Epithelia. J Neurosci 30, 15686–15694. [PubMed: 21084624]

Brann Jessica H., Ellis Deandrea P., Ku Benson S., Spinazzi Eleonora F., and Firestein Stuart. 2015. “Injury in Aged Animals Robustly Activates Quiescent Olfactory Neural Stem Cells.” Frontiers in Neuroscience 9. doi: 10.3389/fnins.2015.00367.

Buschhüter D, Smitka M, Puschmann S, Gerber JC, Witt M, Abolmaali ND, and Hummel T. 2008. “Correlation between Olfactory Bulb Volume and Olfactory Function.” NeuroImage 42(2):498–502. doi: 10.1016/j.neuroimage.2008.05.004. [PubMed: 18555701]

Chen M, Reed RR, and Lane AP (2019). Chronic Inflammation Directs an Olfactory Stem Cell Functional Switch from Neuroregeneration to Immune Defense. Cell Stem Cell 25, 501–513.e5. [PubMed: 31523027]

Child Kevin M., Herrick Daniel B., Schwob James E., Holbrook Eric H., and Jang Woochan. 2018. “The Neuroregenerative Capacity of Olfactory Stem Cells Is Not Limitless: Implications for Aging.” The Journal of Neuroscience: The Official Journal of the Society for Neuroscience 38(31):6806–24. doi: 10.1523/JNEUROSCI.3261-17.2018. [PubMed: 29934351]

Cummings Diana M., Emge Darren K., Small Steven L., and Margolis Frank L.. 2000. “Pattern of Olfactory Bulb Innervation Returns after Recovery from Reversible Peripheral Deafferentation.” Journal of Comparative Neurology 421(3):362–73. doi: 10.1002/(SICI)1096-9861(20000605)421:3<362::AIDCNE5>3.0.CO;2-8. [PubMed: 10813792]

Doty RL, Shaman P, Applebaum SL, Giberson R, Siksorski L, and Rosenberg L. 1984. “Smell Identification Ability: Changes with Age.” Science (New York, N.Y.) 226(4681):1441–43. doi: 10.1126/science.6505700.

Doty Richard L., and Kamath Vidyulata. 2014. “The Influences of Age on Olfaction: A Review.” Frontiers in Psychology 5. doi: 10.3389/fpsyg.2014.00020.

Douek E, Bannister LH, and Dodson HC. 1975. “Recent Advances in the Pathology of Olfaction.” Proceedings of the Royal Society of Medicine 68(8):467–70. [PubMed: 1202479]

Durante Michael A., Kurtenbach Stefan, Sargi Zoukaa B., Harbour J. William, Choi Rhea, Kurtenbach Sarah, Goss Garrett M., Matsunami Hiroaki, and Goldstein Bradley J.. 2020. “Single-Cell Analysis of Olfactory Neurogenesis and Differentiation in Adult Humans.” Nature Neuroscience 23(3):323–26. doi: 10.1038/s41593-020-0587-9. [PubMed: 32066986]

Faedo Andrea, Ficara Francesca, Ghiani Michela, Aiuti Alessandro, Rubenstein John L. R., and Bulfone Alessandro. 2002. “Developmental Expression of the T-Box Transcription Factor T-Bet/TBX21 during Mouse Embryogenesis.” Mechanisms of Development 116(1):157–60. doi: 10.1016/S09254773(02)00114-4. [PubMed: 12128215]

Feng Wen-Hui, Kauer John S., Adelman Lester, and Talamo Barbara R.. 1997. “New Structure, the ‘Olfactory Pit,’ in Human Olfactory Mucosa.” Journal of Comparative Neurology 378(4):443–53. doi: 10.1002/(SICI)1096-9861(19970224)378:4<443::AID-CNE1>3.0.CO;2-2. [PubMed: 9034902]

Féron François, Perry Christopher, McGrath John J., and Mackay-Sim Alan. 1998. “New Techniques for Biopsy and Culture of Human Olfactory Epithelial Neurons.” Archives of Otolaryngology–Head & Neck Surgery 124(8):861. doi: 10.1001/archotol.124.8.861. [PubMed: 9708710]

Gabellec Marie-Madeleine, Panzanelli Patrizia, Sassoè-Pognetto Marco, and Lledo Pierre-Marie. 2007. “Synapse-Specific Localization of Vesicular Glutamate Transporters in the Rat Olfactory Bulb.” European Journal of Neuroscience 25(5):1373–83. doi: 10.1111/j.1460-9568.2007.05400.x. [PubMed: 17425564]

Graziadei PPC, and Samanen DW. 1980. “Ectopic Glomerular Structures in the Olfactory Bulb of Neonatal and Adult Mice.” Brain Research 187(2):467–72. doi: 10.1016/0006-8993(80)90217-6. [PubMed: 7370741]

Håglin Sofia, Berghard Anna, and Bohm Staffan. 2020. “Increased Retinoic Acid Catabolism in Olfactory Sensory Neurons Activates Dormant Tissue-Specific Stem Cells and Accelerates Age-Related Metaplasia.” Journal of Neuroscience 40(21):4116–29. doi: 10.1523/JNEUROSCI.2468-19.2020. [PubMed: 32385093]

Hang Wei, Liu Gang, Han Tong, Zhang Jinling, and Zhang Qiang. 2015. “[A correlation study on olfactory bulb volumes with ages and olfactory function in healthy adults].” Zhonghua Er Bi Yan Hou Tou Jing Wai Ke Za Zhi = Chinese Journal of Otorhinolaryngology Head and Neck Surgery 50(9):744–48. [PubMed: 26696347]

Hinds JW, and McNelly NA. 1981. “Aging in the Rat Olfactory System: Correlation of Changes in the Olfactory Epithelium and Olfactory Bulb.” The Journal of Comparative Neurology 203(3):441–53. doi: 10.1002/cne.902030308. [PubMed: 7320235]

Holbrook Eric H., Iwema Carrie L., Peluso Carolyn E., and Schwob James E.. 2014. “The Regeneration of P2 Olfactory Sensory Neurons Is Selectively Impaired Following Methyl Bromide Lesion.” Chemical Senses 39(7):601–16. doi: 10.1093/chemse/bju033. [PubMed: 25056730]

Holbrook Eric H., Leopold Donald A., and Schwob James E.. 2005. “Abnormalities of Axon Growth in Human Olfactory Mucosa.” The Laryngoscope 115(12):2144–54. doi: 10.1097/01.MLG.0000181493.83661.CE. [PubMed: 16369158]

Holbrook Eric H., Rebeiz Lina, and Schwob James E.. 2016. “Office-Based Olfactory Mucosa Biopsies.” International Forum of Allergy & Rhinology 6(6):646–53. doi: 10.1002/alr.21711. [PubMed: 26833660]

Holbrook Eric H., Mieleszko Szumowski Karen E., and Schwob James E.. 1995. “An Immunochemical, Ultrastructural, and Developmental Characterization of the Horizontal Basal Cells of Rat Olfactory Epithelium.” Journal of Comparative Neurology 363(1):129–46. doi: 10.1002/cne.903630111. [PubMed: 8682932]

Holbrook Eric H., Wu Enming, Curry William T., Lin Derrick T., and Schwob James E.. 2011. “Immunohistochemical Characterization of Human Olfactory Tissue.” The Laryngoscope 121(8):1687–1701. doi: 10.1002/lary.21856. [PubMed: 21792956]

Hoogland PV, Van Den Berg R, and Huisman E. 2003. “Misrouted Olfactory Fibres and Ectopic Olfactory Glomeruli in Normal Humans and in Parkinson and Alzheimer Patients.” Neuropathology and Applied Neurobiology 29(3):303–11. doi: 10.1046/j.1365-2990.2003.00459.x. [PubMed: 12787327]

Huard Josee M. T., Youngentob Steven L., Goldstein Bradley J., Luskin Marla B., and Schwob James E.. 1998. “Adult Olfactory Epithelium Contains Multipotent Progenitors That Give Rise to Neurons and Non-Neural Cells.” Journal of Comparative Neurology 400(4):469–86. doi: 10.1002/(SICI)10969861(19981102)400:4<469::AID-CNE3>3.0.CO;2-8. [PubMed: 9786409]

Hummel T, Kobal G, Gudziol H, and Mackay-Sim A. 2007. “Normative Data for the “Sniffin’ Sticks” Including Tests of Odor Identification, Odor Discrimination, and Olfactory Thresholds: An Upgrade Based on a Group of More than 3,000 Subjects.” European Archives of Oto-Rhino-Laryngology 264(3):237–43. doi: 10.1007/s00405-006-0173-0. [PubMed: 17021776]

Hummel T, Whitcroft KL, Andrews P, Altundag A, Cinghi C, Costanzo RM, Damm M, Frasnelli J, Gudziol H, Gupta N, Haehne A, Holbrook E, Hong SC, Hornung D, Hüttenbrink KB, Kamel R, Kobayashi M, Konstantinidis I, Landis BN, Leopold DA, Macchi A, Miwa T, Moesges R, Mullol J, Mueller CA, Ottaviano G, Passali GC, Philpott C, Pinto JM, Ramakrishnan VJ, Rombaux P, Roth Y, Schlosser RA, Shu B, Soler G, Stjärne P, Stuck BA, Vodicka J, and Welge-Luessen A. 2017. “Position Paper on Olfactory Dysfunction.” Rhinology. Supplement 54(26):1–30. doi: 10.4193/Rhino16.248.

Jang Woochan, Youngentob Steven L., and Schwob James E.. 2003. “Globose Basal Cells Are Required for Reconstitution of Olfactory Epithelium after Methyl Bromide Lesion.” The Journal of Comparative Neurology 460(1):123–40. doi: 10.1002/cne.10642. [PubMed: 12687701]

Kauer JS, and Cinelli AR. 1993. “Are There Structural and Functional Modules in the Vertebrate Olfactory Bulb?” Microscopy Research and Technique 24(2):157–67. doi: 10.1002/jemt.1070240207. [PubMed: 8457727]

Keyhani Keyvan, Scherer Peter W., and Mozell Maxwell M.. 1997. “A Numerical Model of Nasal Odorant Transport for the Analysis of Human Olfaction.” Journal of Theoretical Biology 186(3):279–301. doi: 10.1006/jtbi.1996.0347. [PubMed: 9219668]

Kondo Kenji, Watanabe Kenta, Sakamoto Takashi, Suzukawa Keigo, Nibu Ken-ichi, Kaga Kimitaka, and Yamasoba Tatsuya. 2009. “Distribution and Severity of Spontaneous Lesions in the Neuroepithelium and Bowman’s Glands in Mouse Olfactory Mucosa: Age-Related Progression.” Cell and Tissue Research 335(3):489–503. doi: 10.1007/s00441-008-0739-9. [PubMed: 19142664]

Leopold Donald A., Hummel Thomas, Schwob James E., Seok Chen Hong Michael Knecht, and Kobal Gerd. 2000. “Anterior Distribution of Human Olfactory Epithelium.” The Laryngoscope 110(3):417–21. doi: 10.1097/00005537-200003000-00016. [PubMed: 10718430]

Loo Alice T., Youngentob Steven L., Kent Paul F., and Schwob James E.. 1996. “The Aging Olfactory Epithelium: Neurogenesis, Response to Damage, and Odorant-Induced Activity.” International Journal of Developmental Neuroscience 14(7):881–900. doi: 10.1016/S0736-5748(96)00046-9. [PubMed: 9010732]

de Lorenzo AJ 1957. “Electron Microscopic Observations Of The Olfactory Mucosa And Olfactory Nerve.” The Journal of Biophysical and Biochemical Cytology 3(6):839– 50. [PubMed: 13481018]

Lu Ran, Aziz N. Ahmad, Reuter Martin, Stöcker Tony, and Breteler Monique M. B.. 2021. “Evaluation of the Neuroanatomical Basis of Olfactory Dysfunction in the General Population.” JAMA Otolaryngology– Head & Neck Surgery. doi: 10.1001/jamaoto.2021.2026.

Maresh Alison, Diego Rodriguez Gil Mary C. Whitman, and Greer Charles A.. 2008. “Principles of Glomerular Organization in the Human Olfactory Bulb – Implications for Odor Processing” edited by Hochman S. PLoS ONE 3(7):e2640. doi: 10.1371/journal.pone.0002640. [PubMed: 18612420]

Meisami E, Mikhail L, Baim D, and Bhatnagar KP. 1998. “Human Olfactory Bulb: Aging of Glomeruli and Mitral Cells and a Search for the Accessory Olfactory Bulb.” Annals of the New York Academy of Sciences 855:708–15. [PubMed: 9929675]

Mobley Arie S., Rodriguez-Gil Diego J., Imamura Fumiaki, and Greer Charles A.. 2014. “Aging in the Olfactory System.” Trends in Neurosciences 37(2):77–84. doi: 10.1016/j.tins.2013.11.004. [PubMed: 24361044]

Monti-Graziadei GA, Margolis FL, Harding JW, and Graziadei PP. 1977. “Immunocytochemistry of the Olfactory Marker Protein.” Journal of Histochemistry & Cytochemistry 25(12):1311–16. doi: 10.1177/25.12.336785. [PubMed: 336785]

Mori Kensaku, Nagao Hiroshi, and Yoshihara Yoshihiro. 1999. “The Olfactory Bulb: Coding and Processing of Odor Molecule Information.” Science 286(5440):711–15. doi: 10.1126/science.286.5440.711. [PubMed: 10531048]

Mori Kensaku, and Sakano Hitoshi. 2011. “How Is the Olfactory Map Formed and Interpreted in the Mammalian Brain?” Annual Review of Neuroscience 34(1):467–99. doi: 10.1146/annurev-neuro-112210-112917.

Morrison EE, and Costanzo RM. 1992. “Morphology of Olfactory Epithelium in Humans and Other Vertebrates.” Microscopy Research and Technique 23(1):49–61. doi: 10.1002/jemt.1070230105. [PubMed: 1392071]

Naessen R 1971. “An Enquiry on the Morphological Characteristics and Possible Changes with Age in the Olfactory Region of Man.” Acta Oto-Laryngologica 71(1–6):49–62. doi: 10.3109/00016487109125332. [PubMed: 5100075]

Nakashima T, Tanaka M, Inamitsu M, and Uemura T. 1991. “Immunohistopathology of Variations of Human Olfactory Mucosa.” European Archives of Oto-Rhino-Laryngology: Official Journal of the European Federation of Oto-Rhino-Laryngological Societies (EUFOS): Affiliated with the German Society for Oto-Rhino-Laryngology - Head and Neck Surgery 248(6):370–75.

Nakashima Tadashi, Kimmelman Charles P., and Snow James B.. 1984. “Structure of Human Fetal and Adult Olfactory Neuroepithelium.” Archives of Otolaryngology 110(10):641–46. doi: 10.1001/archotol.1984.00800360013003. [PubMed: 6477257]

Oliva AD, Gupta R, Issa K, Abi Hachem R, Jang DW, Wellford SA, Moseman EA, Matsunami H, and Goldstein BJ (2022). Aging-related olfactory loss is associated with olfactory stem cell transcriptional alterations in humans. J Clin Invest 132, e155506. [PubMed: 34990409]

Omura Kazuhiro, Han Bing, Nishijima Hironobu, Aoki Satoshi, Ebihara Teru, Kondo Kenji, Otori Nobuyoshi, Kojima Hiromi, Yamasoba Tatsuya, and Kikuta Shu. 2021. “Heterogeneous

Distribution of Mature Olfactory Sensory Neurons in Human Olfactory Epithelium." International Forum of Allergy & Rhinology n/a(n/a). doi: 10.1002/alr.22885.

Packard A, Schnittke N, Romano RA, Sinha S, and Schwob JE. 2011. "Np63 Regulates Stem Cell Dynamics in the Mammalian Olfactory Epithelium." Journal of Neuroscience 31(24):8748–59. doi: 10.1523/JNEUROSCI.0681-11.2011. [PubMed: 21677159]

Paik SI, Lehman MN, Seiden AM, Duncan HJ, and Smith DV. 1992. "Human Olfactory Biopsy: The Influence of Age and Receptor Distribution." Archives of Otolaryngology - Head and Neck Surgery 118(7):731–38. doi: 10.1001/archotol.1992.01880070061012. [PubMed: 1627295]

Richard MB, Taylor SR, and Greer CA. 2010. "Age-Induced Disruption of Selective Olfactory Bulb Synaptic Circuits." Proceedings of the National Academy of Sciences 107(35):15613–18. doi: 10.1073/pnas.1007931107.

Rosli Y, Breckenridge LJ, and Smith RA. 1999. "An Ultrastructural Study of Age-Related Changes in Mouse Olfactory Epithelium." Journal of Electron Microscopy 48(1):77–84. [PubMed: 10101872]

Schwob James E. 2002. "Neural Regeneration and the Peripheral Olfactory System." The Anatomical Record 269(1):33–49. doi: 10.1002/ar.10047. [PubMed: 11891623]

Schwob James E., Youngentob Steven L., and Meiri Karina F.. 1994. "On the Formation of Neuromata in the Primtary Olfactory Projection." Journal of Comparative Neurology 340(3):361–80. doi: 10.1002/cne.903400307. [PubMed: 8188856]

Smith Robin L., Baker Harriet, Kolstad Kaare, Spencer Dennis D., and Geer Charles A.. 1991. "Localization of Tyrosine Hydroxylase and Olfactory Marker Protein Immunoreactivities in the Human and Macaque Olfactory Bulb." Brain Research 548(1):140–48. doi: 10.1016/0006-8993(91)91115-H. [PubMed: 1678294]

Treloar Helen B., Feinstein Paul, Mombaerts Peter, and Greer Charles A.. 2002. "Specificity of Glomerular Targeting by Olfactory Sensory Axons." Journal of Neuroscience 22(7):2469–77. doi: 10.1523/JNEUROSCI.22-07-02469.2002. [PubMed: 11923411]

Trojanowski John Q., Newman Paul D., Hill William D., and Lee Virginia M. Y.. 1991. "Human Olfactory Epithelium in Normal Aging, Alzheimer's Disease, and Other Neurodegenerative Disorders." Journal of Comparative Neurology 310(3):365–76. doi: 10.1002/cne.903100307. [PubMed: 1723988]

Vennemann MM, Hummel T, and Berger K. 2008. "The Association between Smoking and Smell and Taste Impairment in the General Population." Journal of Neurology 255(8):1121–26. doi: 10.1007/s00415-008-0807-9. [PubMed: 18677645]

Witt Martin, Bormann Katja, Gudziol Volker, Pehlke Kerstin, Barth Kathrin, Minovi Amir, Antje Hähner Heinz Reichmann, and Hummel Thomas. 2009. "Biopsies of Olfactory Epithelium in Patients with Parkinson's Disease." Movement Disorders 24(6):906–14. doi: 10.1002/mds.22464. [PubMed: 19205070]

Xie Fang, Fang Cheng, Schnittke Nikolai, Schwob James E., and Ding Xinxin. 2013. "Mechanisms of Permanent Loss of Olfactory Receptor Neurons Induced by the Herbicide 2,6-Dichlorobenzonitrile: Effects on Stem Cells and Noninvolvement of Acute Induction of the Inflammatory Cytokine IL-6." Toxicology and Applied Pharmacology 272(3):598–607. doi: 10.1016/j.taap.2013.07.020. [PubMed: 23921153]

Zapiec Bolek, Dieriks Birger V., Tan Sheryl, Faull Richard L. M., Mombaerts Peter, and Curtis Maurice A.. 2017. "A Ventral Glomerular Deficit in Parkinson's Disease Revealed by Whole Olfactory Bulb Reconstruction." Brain 140(10):2722–36. doi: 10.1093/brain/awx208. [PubMed: 28969383]

Zhang Chenping, and Wang Xiaochun. 2017. "Initiation of the Age-Related Decline of Odor Identification in Humans: A Meta-Analysis." Ageing Research Reviews 40:45–50. doi: 10.1016/j.arr.2017.08.004. [PubMed: 28830800]

Key points:

1. A gradual loss of olfactory sensory neurons with age in human olfactory epithelium is also reflected in a reduction in glomeruli within the olfactory bulb.
2. This gradual loss of neurons and synaptic connections with age occurs in a specific, spatially inhomogeneous manner.
3. Decreasing mitotically active olfactory epithelium basal cells may contribute to age-related neuronal decline and smell loss in humans.

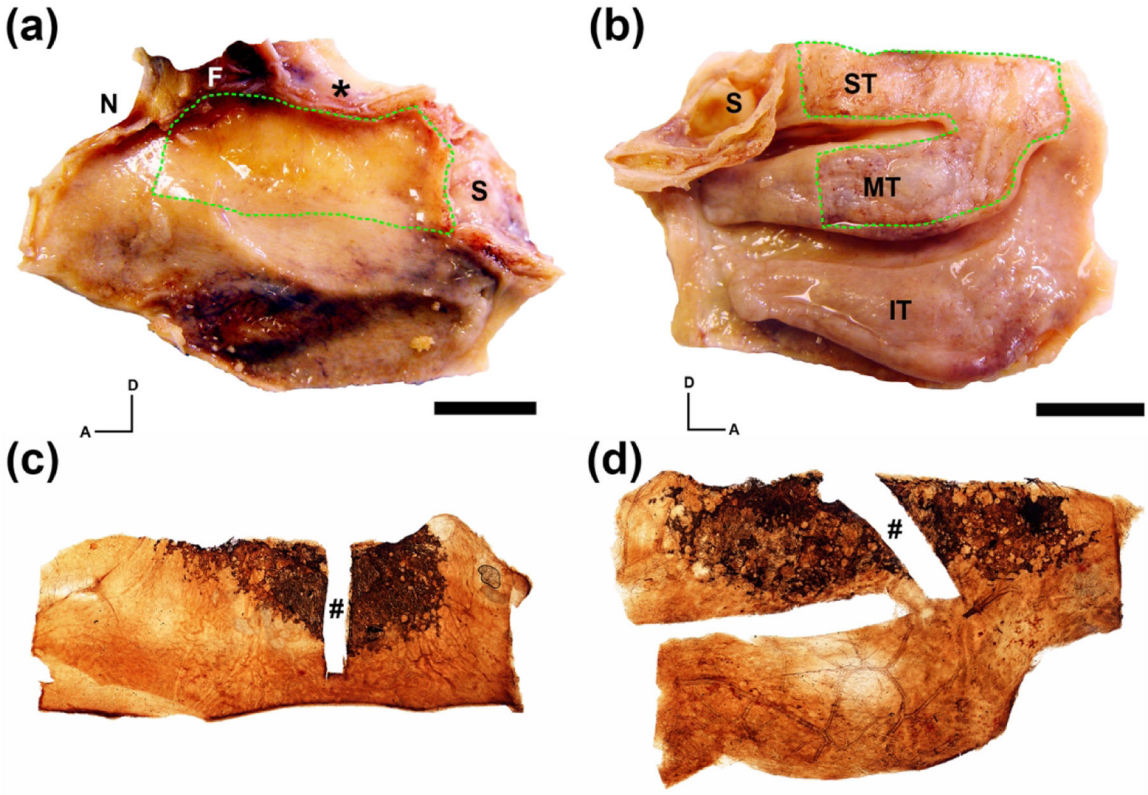

Figure 1.

Generation of whole mucosal neuronal staining obtained from an 80 year-old male. The left nasal cavity autopsy specimen was split longitudinally along the cribriform plate (**asterisk**) exposing the septal surface **(a)** and lateral surface **(b)**. **(a, b)**. Whole mucosal sheets encompassing the region of olfactory mucosa were removed from the specimen (green dashed line). **(c, d)**. Immunohistochemical staining of the excised septal **(c)** and lateral **(d)** mucosal sheets using anti-beta III tubulin (TUJ1) with DAB as a chromogen reveal brown neuronal staining of the olfactory receptor neurons at the dorsal portion of the specimens. A rectangular portion of the mucosal sheets used for sectioning and further histologic analysis was excised prior to whole mount staining (#). **A** = anterior; **D** = dorsal; **F** = frontal sinus; **N** = nasal bone; **S** = sphenoid sinus; **IT** = inferior turbinate; **MT** = middle turbinate; **ST** = superior turbinate; **scale bars** = 15 mm.

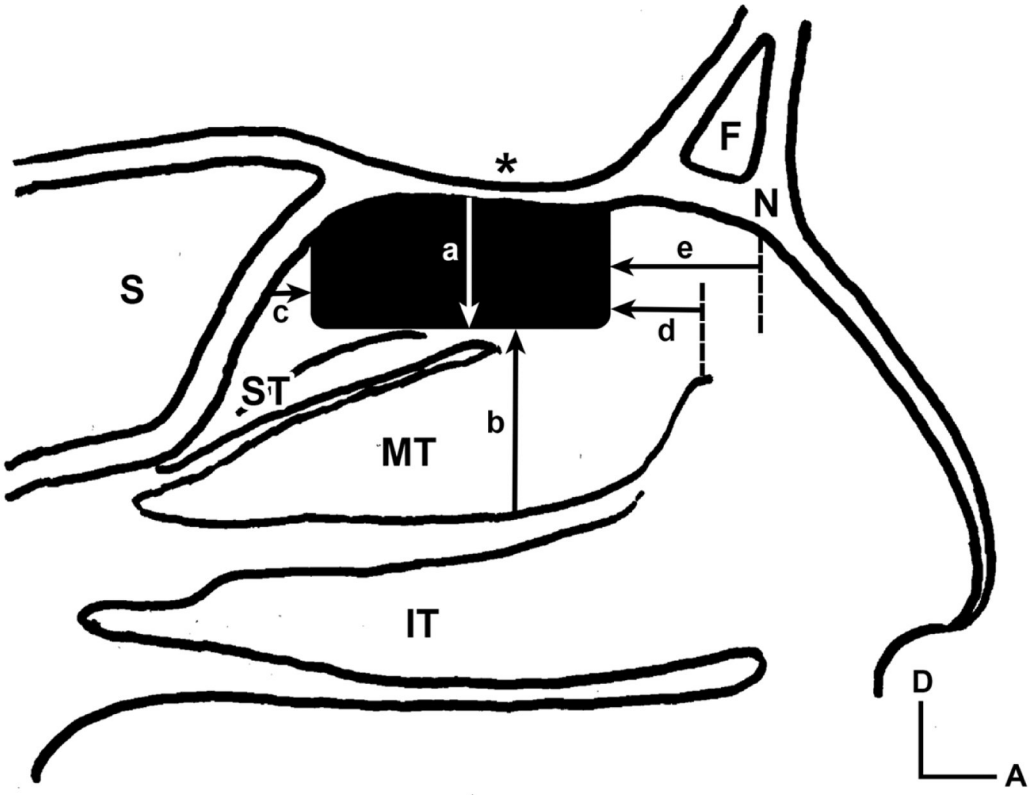

Lateral Measurements (mm)	n	Mean	SEM	Max	Min
a - cribriform to inferior edge	28	10.40	0.47	14.95	6.26
b - inferior MT to inferior edge	27	17.25	0.83	25.50	11.03
c - sphenoid to posterior edge	33	3.74	0.67	16.03	0
d - anterior MT to anterior edge	25	7.27	1.01	17.91	(-) 3.04
Septum Measurements (mm)	**n**	**Mean**	**SEM**	**Max**	**Min**
a - cribriform to inferior edge	34	10.02	0.42	14.66	4.94
c - sphenoid to posterior edge	36	3.50	0.53	10.61	0
e - nasion to anterior edge	33	12.03	1.14	28.33	1.36

Figure 2.

Average position of the olfactory epithelium (OE) in relation to anatomic structures of the nasal cavity. The **solid black rectangular shape** depicts the average location of neuronal stained OE just below the cribriform plate (**asterisk**) in a sagittal illustration of the nasal cavity. **Arrows** demonstrate measurements performed on stained specimens with corresponding average values listed in the **table**: **a** = distance from the cribriform plate to the inferior boarder of OE; **b** = distance from the inferior boarder of the middle turbinate to the inferior boarder of the OE; **c** = distance from the face of the sphenoid sinus to the posterior boarder of the OE; **d** = distance from the anterior middle turbinate attachment to the anterior boarder of the OE; **e** = distance from the under surface of the nasion to the anterior OE.

A = anterior; **D** = dorsal; **F** = frontal sinus; **N** = nasion; **S** = sphenoid sinus; **IT** = inferior turbinate; **MT** = middle turbinate; **ST** = superior turbinate

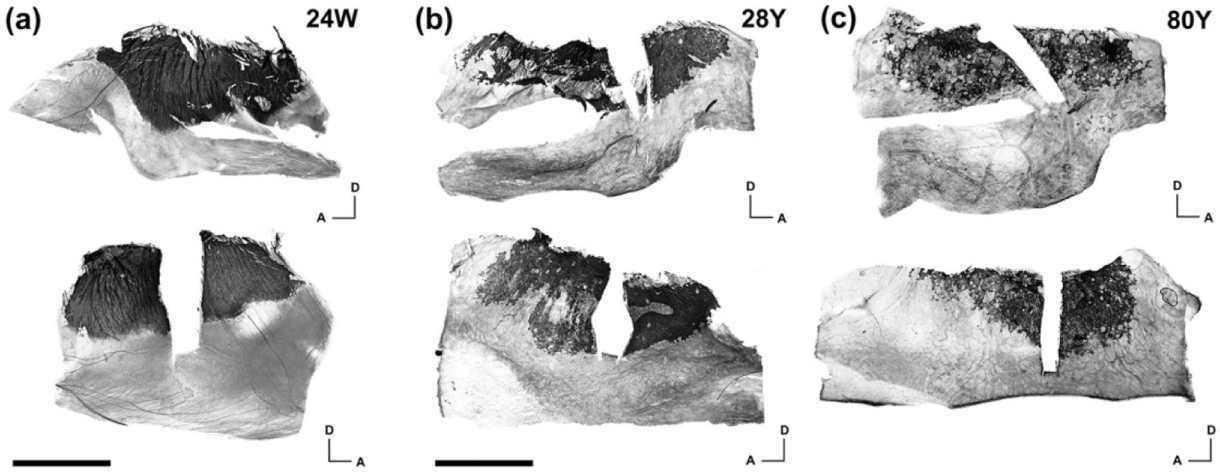

OE Area (cm x cm)	n	Mean	SEM	Max	Min	P-value
R Septum	14	1.47	0.199	3.558	0.735	0.487
L Septum	12	1.24	0.206	2.996	0.334	
R Lateral	7	1.795	0.195	2.852	1.401	0.696*
L Lateral	9	1.669	0.232	2.937	0.717	
Septum Combined	26	1.366	0.142	3.558	0.334	0.043
Lateral Combined	16	1.724	0.152	2.937	0.717	

OE Remaining (%)	n	Mean	SEM	Max	Min	P-value
R Septum	15	74.5	3	94	55.4	0.448*
L Septum	13	71.2	3.7	94.1	44.9	
R Lateral	7	67.9	6.7	95.8	45.2	0.424*
L Lateral	13	73.1	3.2	95.4	54.7	
Septum Combined	28	72.9	2.3	94.1	44.9	0.664*
Lateral Combined	20	71.3	3	95.8	45.2	

* passed normality test

Figure 3.

The adult olfactory epithelium decreases in area and decreases in olfactory neuronal density with age. **(a)**. A whole mount staining of the lateral (top) and septal (bottom) mucosa from the right nasal cavity of a human female embryo at 24 weeks gestation using TUJ1 antibodies reveals a distinct boarder of dark stained OE with respiratory epithelium (RE). In addition, the OE region is stained as a complete sheet of neurons without patches of absent staining. **Scale bar** = 5 mm. **(b)**. Whole mount staining of mucosa from the left nasal cavity of a 28 year-old male demonstrates an irregular boarder of OE with RE and appearance of multiple patches within the OE that lack staining. **(c).** With increased age there appears to be a greater disruption of the OE and RE boarder and appearance of a greater number of patches within the OE absent of neuronal staining as demonstrated by the whole mount staining of mucosal from the left nasal cavity of an 80 year-old male. **Scale bar** for **(b)** and **(c)** = 10 mm. **A** = anterior; **D** = dorsal. **(d)**. Measurements of the area stained for neurons in septum and lateral mucosal specimens are plotted as a function of age. Given the known association of age with smell loss and dementia, multiple linear regression was used to assess for correlation of age with OE area. Regression lines demonstrate a more pronounced reduction with age in septal mucosa compared with lateral mucosa. The associated table

shows average OE area values that are significantly decreased on the septum compared with the lateral side. **(e)**. Measurements of the remaining stained neurons within the boundary of OE as a percent of the entire area are plotted as a function of age. In both the septum and lateral mucosa there is a decrease in neuronal staining within the OE area with age. Unlike the OE area measurements, there was no difference in percent neuronal staining between septum and lateral mucosa. **SEM** = standard error of the mean.

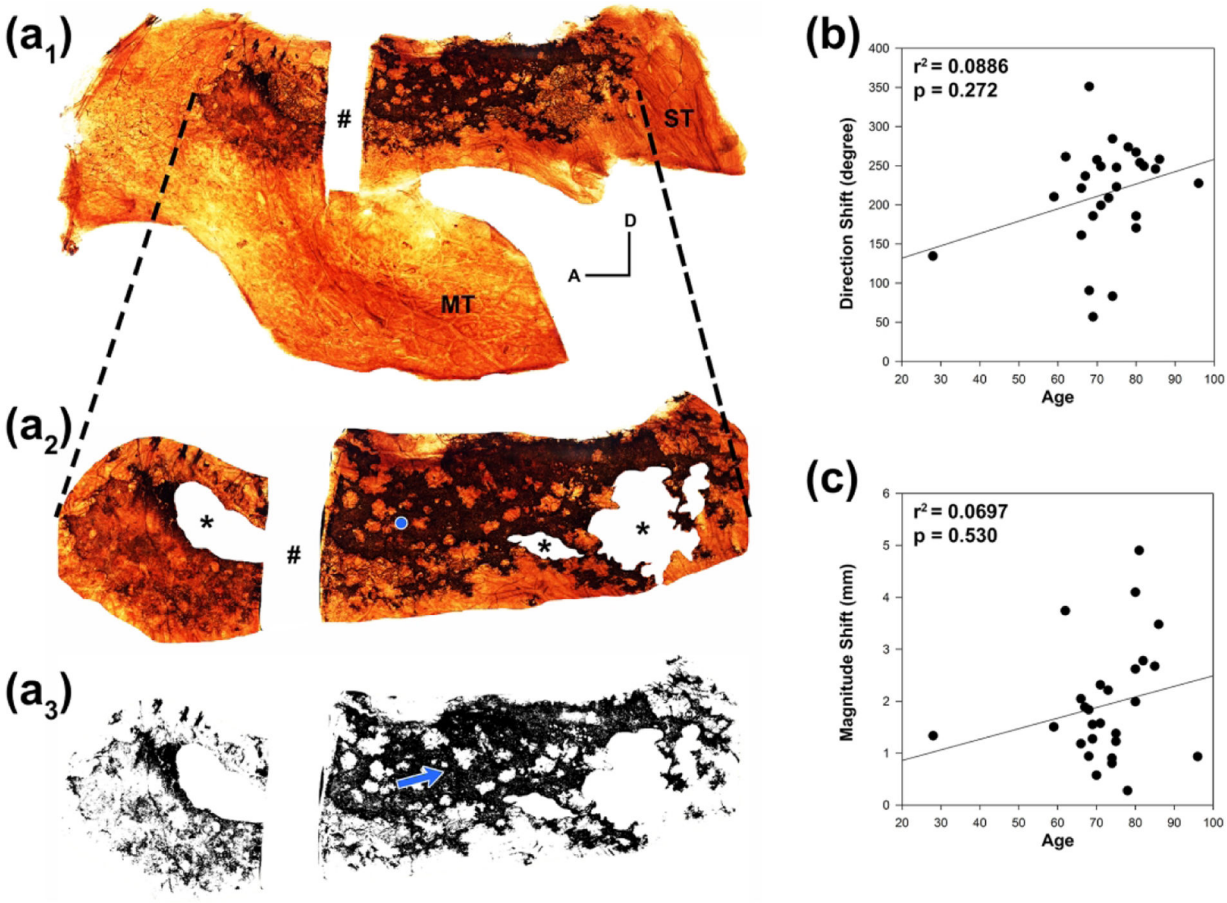

Figure 4.

There is a higher density of neurons in the posterior and dorsal region of adult OE. (**a_1**). Whole mount neuronal staining of the right lateral mucosa from an 86 year-old female reveals brown DAB labeled OE with irregular boarders and patchy regions of absent staining. A rectangular area of mucosa (**#**) was removed for sectioning and further immunohistochemistry. To calculate the shift in centroid of remaining olfactory neurons that results from patchy loss within the OE (neuronal centroid), the region of OE is first defined **(a_2)** and portions of the mucosa where the epithelial surface was stripped during processing are removed from analysis (**asterisks**). The center of the remaining geometric shape (areal centroid) is mathematically calculated and shown with a **blue dot**. The **dashed lines** represent corresponding edges of the OE region extrapolated from **(a_1)**. The adult OE region is not a continuous sheet of olfactory neurons as is seen in embryonic tissue, and the resulting shape generated from remaining olfactory neurons within the OE area **(a_3)** is not equally spaced throughout. The neuronal centroid shifts from the areal centroid toward a region of higher neuronal density (**blue arrow**). **A** = anterior; **D** = dorsal; **MT** = middle turbinate; **ST** = superior turbinate. **(b)**. The degree direction of the centroid shift when compared to age appears to increase with a linear regression plot but is not found to be statistically significant with multiple linear regression considering additional effects of dementia. **(c)**. Similarly, the magnitude of the centroid shift appears to increase with age but was not statistically significant.

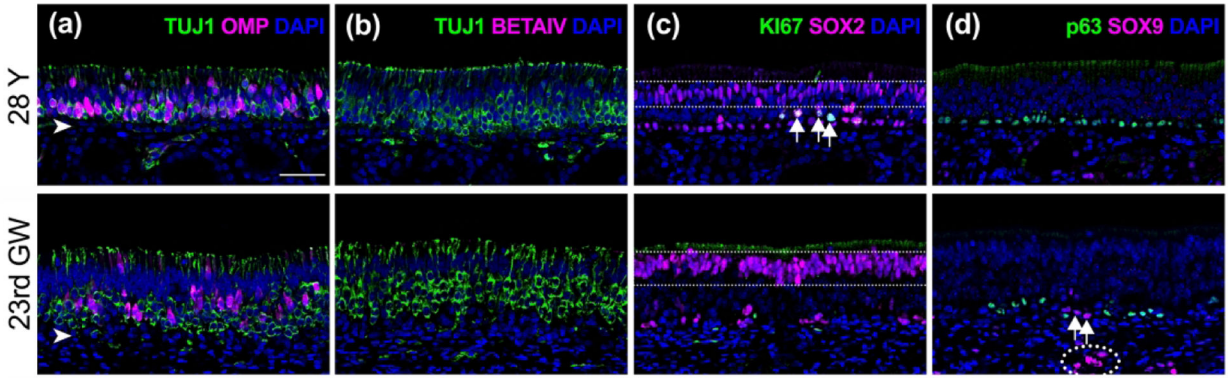

Figure 5.

Comparison of fetal and healthy adult olfactory epithelium. Adjacent sections obtained from vertical rectangular strips of olfactory mucosa from a young-adult male (#12-080313, 28 years (Y), **top row**) and male embryo (#6167, 23rd gestation week (GW), **bottom row**) were labeled with immunofluorescence to identify specific cell types within the epithelium. **(a)**. A pseudostratified columnar neuronal epithelium is observed in both samples with abundant neurons labeled **green** using anti-ß-tubulin III (TUJ1). A subset of neurons are co-labeled with the mature olfactory neurons marker, OMP (**magenta**). In embryonic tissue, the OE consistently demonstrates a slightly thicker neuronal layer compared to healthy adult tissue. **(b)**. Respiratory metaplasia identified with antibodies against ß-tubulin IV (BetaIV, **magenta**) is absent in regions of healthy OE and all embryonic OE sections but occurs frequently in adult OE (see Figure 7). **(c)**. Horizontal basal cells (HBCs), globose basal cells (GBCs), and supporting cells are labeled with antibodies against SOX2 (**magenta**). In both adult and embryonic sections, HBCs appear in a single row along the basal lamina and rarely co-label with antibodies against the cell division marker KI67 (**green**). SOX2(+) GBCs positioned just above the HBCs (**arrows**) actively proliferate and are often grouped in clusters in adult tissue. In fetal tissue, dividing basal cells are rarely found. A palisade of supporting cell nuclei labeled with SOX2 is seen at the apical level in both adult and fetal OE (**dotted rectangle**). **(d)**. HBCs labeled with anti-p63 antibodies (**green**) are observed in a linearly arrayed uniform basal layer in adult OE as opposed to a discontinuous fashion observed in fetal tissue. SOX9(+) duct/gland cells (**magenta**) appear in the lamina propria in both young-adult and fetal OE (**dotted circle**). Their associated duct cells can be found traversing the basal lamina (**arrows**). **Scale bar** = 50 μm.

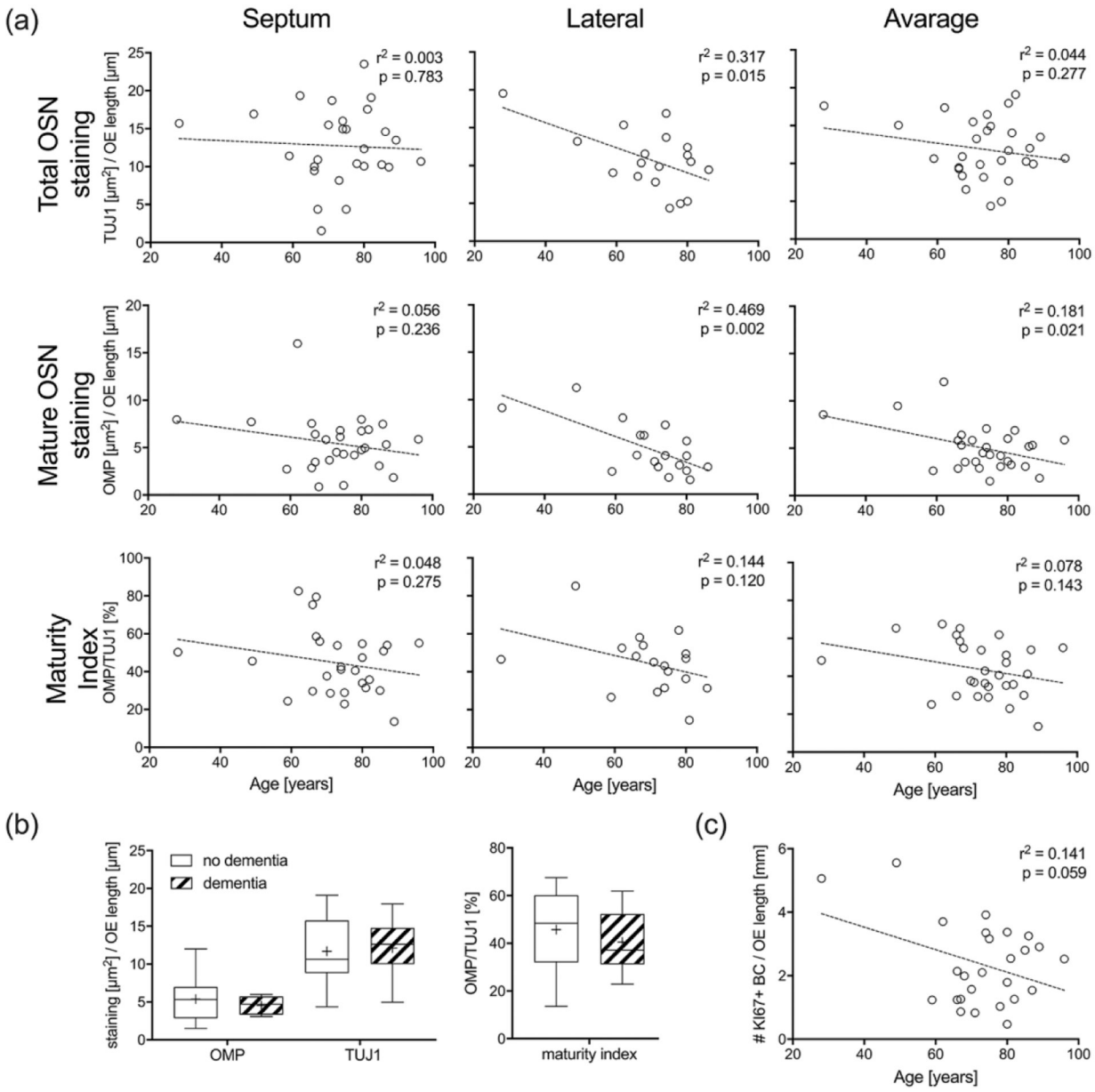

Figure 6.

Amount of mature OSNs decreases significantly with age. **(a)**. Average amount staining from three sections through each mucosal strip taken from the septum (n = 27) and lateral wall (n = 18) below the cribriform plate were normalized to the length of OE. Linear regression curves are superimposed on scatter plots of staining versus age. Separate analyses for the septum, lateral wall, and average of both are provided for total OSNs (TUJ1 labeling), mature OSNs (OMP labeling), and maturity index (% epithelial labeling of OMP/TUJ1). **(b)**. Boxplots of total OSNs, mature OSNs and OSN maturity index across mucosal strips obtained from the septum (n = 27) and lateral wall (n = 18) in respect to the presence or absence of dementia did not reveal significant differences. **(c)**. Average number

of dividing KI67(+)/SOX2(+) basal cells from three sections through each mucosal strip taken from the septum (n = 27) compared with age is shown using a linear regression curve.

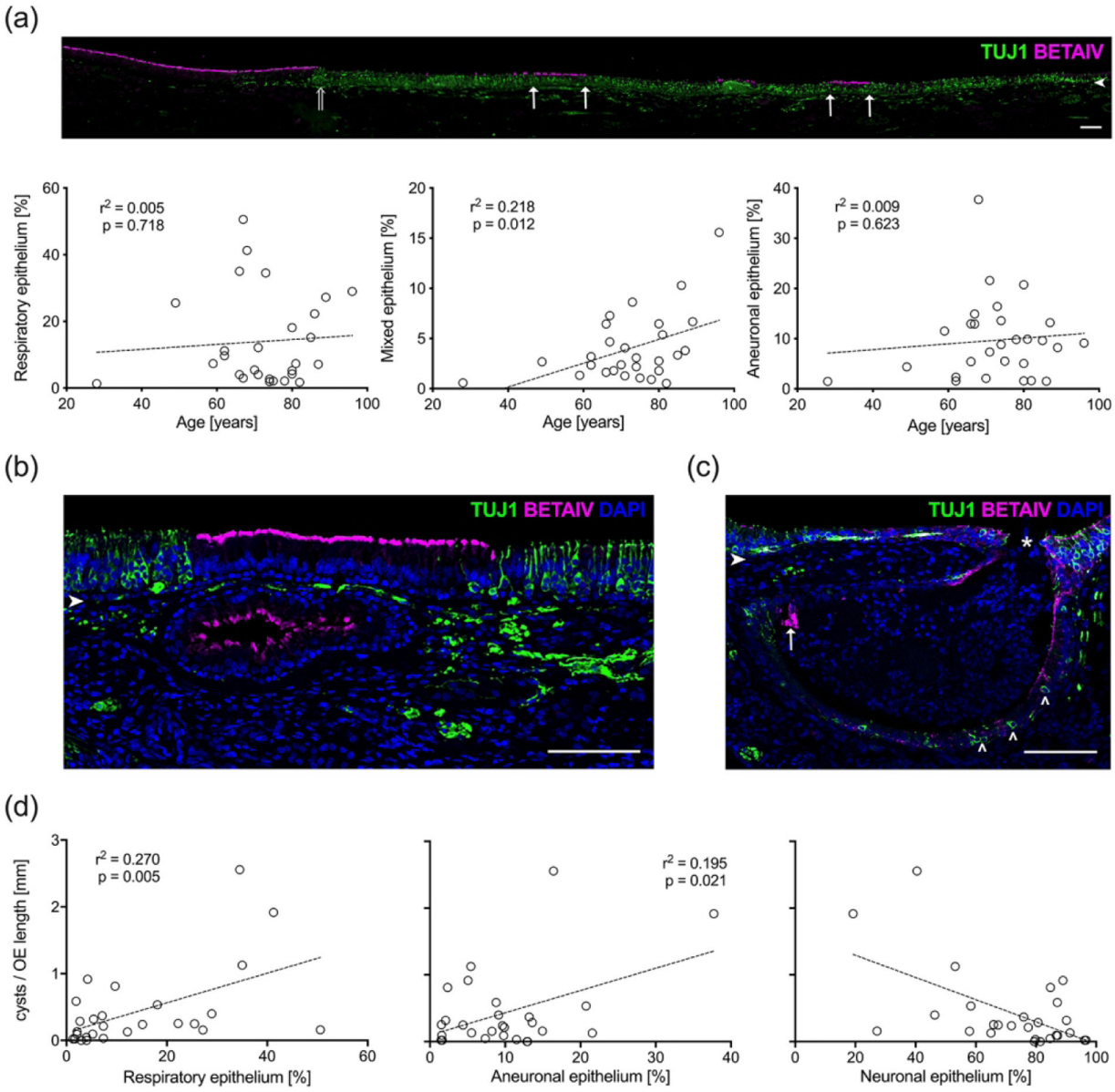

Figure 7.

Epithelial metaplasia and characteristics of subepithelial cysts correlate with age. **(a)**. A mosaic image of a representative adult section of olfactory mucosa (#11-09008, 81 year male, left septum) stained for TUJ1(+) neurons (**green**) and Beta-IV(+) respiratory cilia (**magenta**) reveals regions of mixed epithelium (boarders defined by **arrows**). The transition from respiratory epithelium and OE is seen on the left (**open arrow**). **Scale bar** = 100 μm. The length of Beta-IV(+)/TUJ1(−) respiratory patches, Beta-IV(+)/TUJ1(+) mixed patches, and BetaIV(−)/TUJ1(−) aneuronal patches were normalized to the entire OE length and averaged across three equally spaced sections obtained from right and left septal mucosal strips (n = 28). Scatterplots and linear regression curves were generated as a function of age for each epithelial type. The amount of mixed epithelium correlates with advancing age. **(b)**. A section from a 62-year-old man (#10–08058, right septum) displays a respiratory

epithelia-lined submucosal cyst with Beta-IV(+) (**magenta**) staining of the respiratory cilia. Note the overlying epithelium is also respiratory and flanked by normal OE containing TUJ1(+) (**green**) OSNs. **Scale bar** = 100 μm. **(c)**. A section from an 87-year-old male specimen (#08-06004, left septum) provides an example of a mixed cyst with TUJ1(+) neurons (**open arrowheads**) and a small area of Beta-IV(+)-respiratory epithelium (**arrow**) that appears to erupt through the thin overlying epithelial surface (**asterisk**). **Scale bar** = 100 μm. **Arrowheads** in **(a)**, **(b)**, and **(c)** indicate the basal lamina. **(d)**. Number of cysts with true epithelial lining correlates with amount of neuronal impoverished epithelia. The total number of cysts were counted and normalized to the OE-length then averaged across three evenly spaced sections from separate septal mucosal strips (n = 28). The number of cysts per length of OE was then compared with the percent length of respiratory, neuronal and aneuronal epithelium within the OE. Corresponding scatterplots and linear regression curves reveal higher number of submucosal cysts in OEs that have higher percentages of respiratory and aneuronal epithelium. A higher percentage of neuroepithelium is related with lower number of cysts.

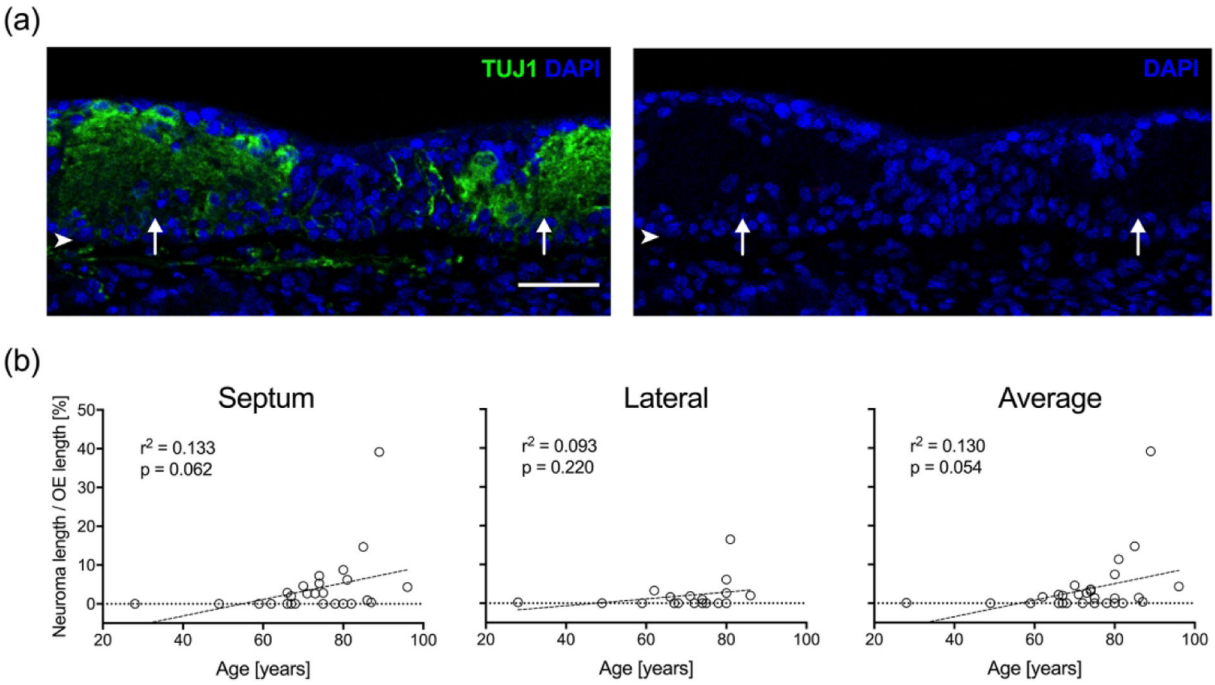

Figure 8.

OE neuromas increase with age. **(a)**. A section of OE from an 81-year-old male specimen (#11-09008, right septum) stained with anti-TUJ1 antibody (**green**) labels neuromas (**arrows**) within the epithelium. The area occupied by the neuromas is acellular and filled with dystrophic neurites lacking the DAPI nuclear staining (**blue**). **Scale bar** = 100 μm; **arrowheads** indicate the basal lamina. **(b)**. The average cumulative length of neuromas per total OE length [%] calculated for septal and lateral mucosal strips as well as the combined septal and lateral mucosal strips from each specimen was compared with age. Scatter plots and linear regression curves demonstrate a strong trend toward increasing percent length with neurons as a function of increasing age.

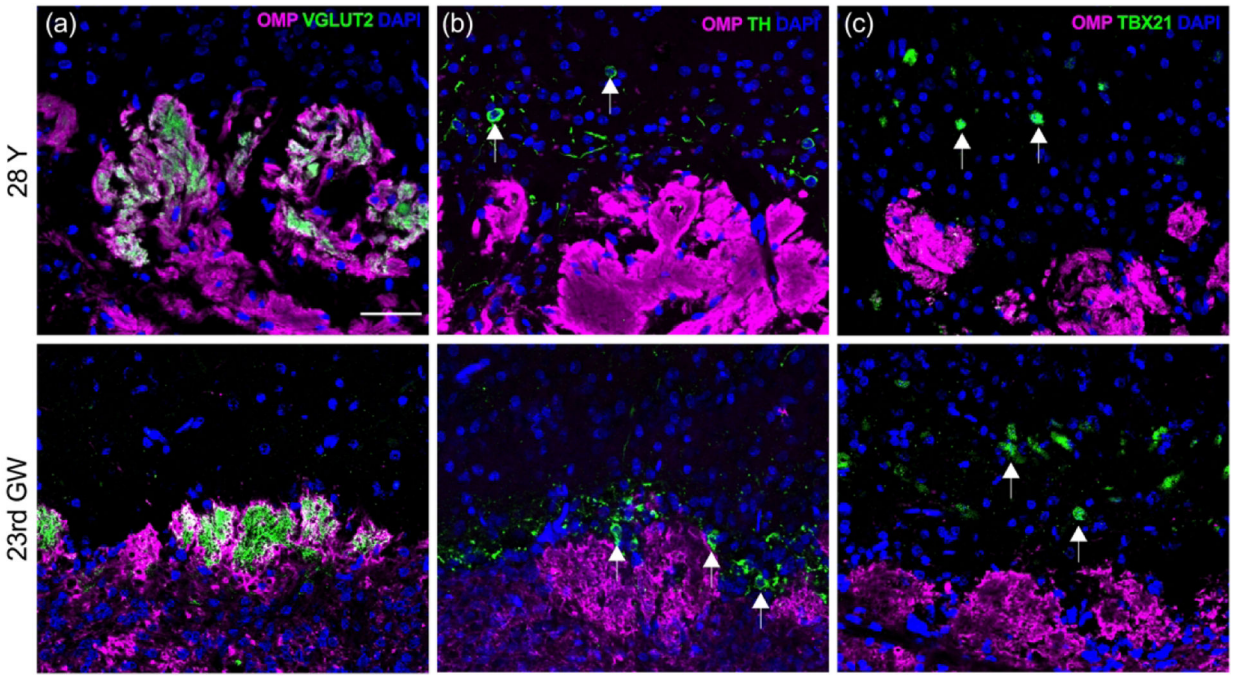

Figure 9.

OB glomeruli appear more disorganized with age. Near-adjacent coronal sections were obtained through the OB from a young-adult (#12-080313, 28 years old (**28Y**, male; **top row**) and embryo (#6167, 23rd gestation week (**23rd GW**), male; **bottom row**). **(a)**. The OSN axon processes of the olfactory nerve layer at the periphery of the OB (oriented at the bottom of each panel) are labeled with antibodies to OMP (**magenta**). Terminal synapses with second order neurons are identified with antibodies against vesicular glutamate transporter type 2 (VGLUT2, **green**) within glomerular neuropil units. While fetal glomeruli appear as small buds just beginning to form into more robust structures, adult glomeruli are larger, more difficult to identify as discrete units, and often extend into deeper regions (see Fig 10(a) for lower magnification). **(b)**. Adult periglomerular cells (**arrows**) labeled with antibodies against tyrosine hydroxylase (TH, **green**) are comparable in their position surrounding individual glomeruli in both adult and fetal tissue, but in embryonic tissue they appear closer to glomeruli. **(c)**. Mitral cells (**arrows**) are labeled with anti-TBX21 antibodies (**green**). In adult OB they appear greatly reduced in number and somewhat sporadic while embryonic mitral cells demonstrate an established uniform layer located in a zone deep to the glomeruli as described in rodent OB. **Scale bar** = 50 μm.

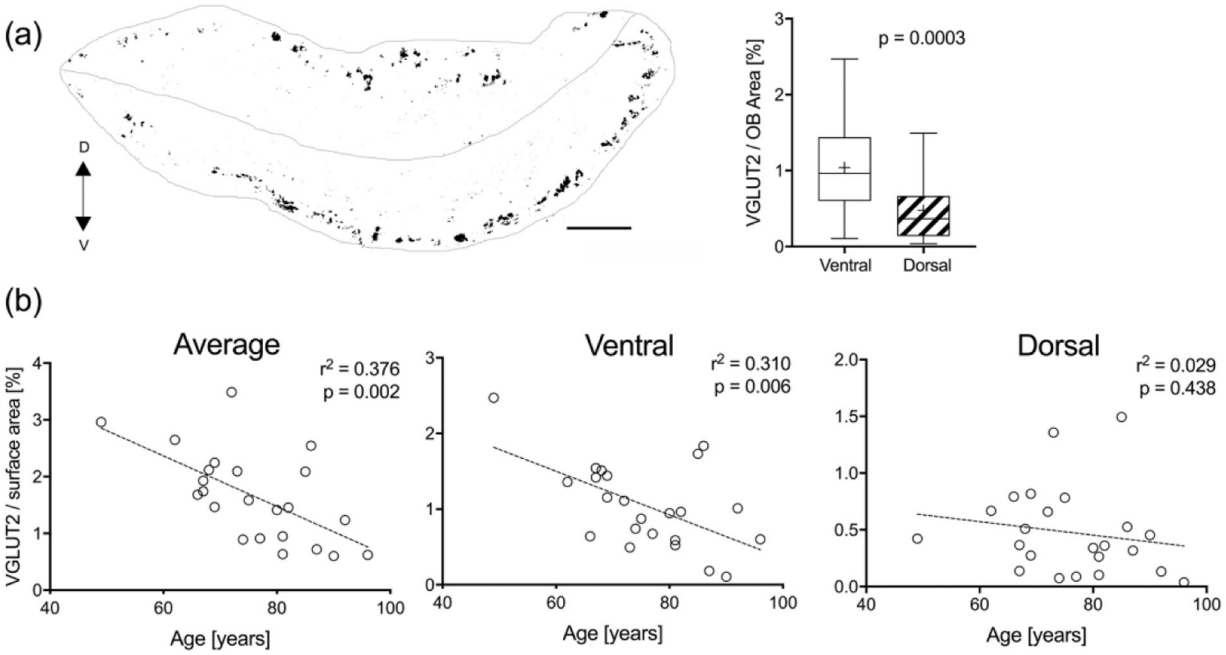

Figure 10.

Amount of VGLUT2(+) glomerular staining varies with OB region and age. **(a)**. A schematic generated from a mosaic image of a coronal section through the OB of a 75 year-old male (#07-08032, left bulb) stained with VGLUT2 (**black**) to identify glomeruli. A line through the middle dissects the OB section into a dorsal (**D**) and ventral (**V**) half (**scale bar** = 0.5 mm). The average percent area of positive VGLUT2-staining in the ventral and dorsal half of the OBs was compared across all specimens (n = 23). Boxplots demonstrate significantly more glomerular staining in the ventral half. **(b)**. Average percent glomerular staining was compared with age. Linear regression curves showed the total amount of glomerular staining per bulb decreases with age and appears to be related to a decline in ventral glomeruli while the dorsal portion remains relatively stable.

J Comp Neurol. Author manuscript; available in PMC 2023 August 01.

Table 1.

Case information

Specimen	Source	Tissue	Age [Y]	Sex	Cause of Death	Comorbidities
07-08032	NDRI	OB, OE	75	M	Alzheimer's	Emphysema, nicotine abuse
07-08073	NDRI	OB, OE	85	F	Alzheimer's	Arthritis, CVA, HTN
07-09010	NDRI	OE	78	M	CAD	Nicotine abuse, pulmonary artery disease
07-12056	NDRI	OE	70	M	Alzheimer's	Arthritis, cerebral palsy, epilepsy, HTN
08-01034	NDRI	OE	75	M	Lung cancer	Arthritis, emphysema, HTN, TIA
08-01041	NDRI	OE	78	F	Dementia	CVA, epilepsy, HTN
08-01056	NDRI	OB	69	M	Parkinson's	Kidney stones
08-02048	NDRI	OB	90	M	CVA	EtOH abuse, MI
08-06004	NDRI	OB, OE	87	M	Failure to thrive	Arthritis, dementia, epilepsy, pacemaker
08-06020	NDRI	OB, OE	82	F	CHF	Arthritis, cardiomyopathy, MI, pneumonia
08-06069	NDRI	OB	77	M	CVA	Nicotine abuse, pneumonia
08-07007	NDRI	OE	66	F	Liver failure	Liver transplantation, NIDDM, pneumonia
08-08026	NDRI	OE	89	F	Perforated bowel	CHF, HTN, TIA
08-08061	NDRI	OB, OE	96	F	Dementia	Arthritis, colon metastases, HTN, nicotine abuse
08-12002	NDRI	OE	80	M	Pneumonia	CAD, dementia
09-02047	NDRI	OB, OE	49	M	Brain cancer	HTN, depression
09-04005	NDRI	OB, OE	67	F	Lung cancer	Nicotine abuse, vascular disease
10-08058	NDRI	OB, OE	62	M	CHF	HTN, gastrointestinal ulcer, MI, nicotine abuse, reflux
10-09032	NDRI	OB, OE	72	M	CHF	COPD, emphysema, DM, HTN, TIA, renal cancer
11-05019	NDRI	OB, OE	73	M	Lung cancer	Arthritis, CAD, HTN, lung metastases, nicotine abuse
11-06002	NDRI	OB, OE	68	M	ALS	Depression, HTN, nicotine abuse, skin melanoma
11-06054	NDRI	OE	71	M	Lung cancer	Diverticulitis, nicotine abuse, prostate cancer
11-06062	NDRI	OE	59	F	Malignant melanoma	Asthma, CHF, depression, HTN, metastases
11-07033	NDRI	OE	71	F	Dementia	Arthritis, depression, GERD, gout, HTN, osteoporosis, ulcer
11-07034	NDRI	OB, OE	67	M	Lung cancer	Metastases, NIDDM, nicotine abuse
11-07060	NDRI	OB, OE	66	M	Heart Failure	CHF, EtOH abuse, MI, nicotine abuse, RA, GERD
11-08018	NDRI	OB, OE	86	F	Alzheimer's	Arthritis, DM type 1, HTN, mild EtOH abuse, nicotine abuse, renal failure
11-08047	NDRI	OB, OE	74	M	CVA/stroke	Bradycardia with pacer, dementia, hip fracture, moderate EtOH abuse, nicotine abuse, paralysis, pneumonia

Specimen	Source	Tissue	Age [Y]	Sex	Cause of Death	Comorbidities
11-09008	NDRI	OB, OE	81	M	Dementia	DM type 2, HTN, MI, osteoarthritis
11-12010	NDRI	OB	69	F	Failure to thrive	A-fib, brain aneurysm, CVA, HTN, stroke
11-12037	NDRI	OB, OE	80	M	CHF	CHF, CVA, DM type 1, EtOH abuse, MI, nicotine abuse,
12-01063	NDRI	OB	92	M	Cardiovascular disease	Dementia, depression, nicotine abuse
12-02035	NDRI	OB	81	M	Dementia	Bowel resection, dementia, depression
12-02054	NDRI	OE	74	F	Lung cancer with metastases	Metastases to CSF, nicotine abuse, GERD
12-06054	NDRI	OE	80	M	Alzheimer's	Arthritis, CVA, GERD, pneumonia, hydrocephalus
12-080313	AGR	OE	28	M	Demyelinating syndrome	Diabetes insipidus, hearing loss, multiple sclerosis, paraplegic, seizure
9993	ABR	OB, OE	23 GW	M		
6167	ABR	OE	22 GW	M		

Abbreviations: **ABR –** Advanced Bioscience Resources Incorporation; **A-fib –** atrial fibrillation; **AGR –** Anatomy Gifts Registry, Hanover, MD, Alameda, CA; **ALS –** amyotrophic lateral sclerosis; **CAD –** coronary artery disease; **CHF –** congestive heart failure; **COPD –** chronic obstructive pulmonary disease; **CSF –** cerebrospinal fluid; **CVA –** cerebrovascular accident; **DM –** diabetes mellitus; **GERD –** gastroesophageal reflux disease; **GW –** gestation week; **HTN –** hypertension; **MI –** myocardial infarction; **NDRI –** National Research Interchange, Philadelphia, PA; **NIDDM –** non insulin-dependent diabetes mellitus; **OB –** olfactory bulb; **OE –** olfactory epithelium; **RA –** rheumatoid arthritis; **TIA –** transient ischemic attack

Table 2.

Immunohistochemical Staining Conditions

Primary Antibody	Immunogen	Source and Catalog No.	RRID	Species	Antibody Concentration and Amplification	Labeled Cell Types	Specificity Determination
Beta IV tubulin	Synthetic peptide	Abcam (ab179509)	AB_2716759	Rabbit	1:1000 2°	RE sus cells	[1] (Child et al., 2018)
KI67	Synthetic peptide from C-terminus of human Ki-67	Epitomics (4203-1)	AB_765010	Rabbit	1:300 3°	Proliferating cells	[1] (Holbrook et al., 2011)
OMP	Amino acids 1-163 representing full length OMP of human origin	Santa Cruz Biotechnology (sc-365818)	AB_10842164	Mouse	1:100 2°	Mature OSNs	[1] (Child et al., 2018)
OMP	Recombinant full-length protein	Abcam (ab183947)	AB_2858281	Rabbit	1:700 2°	Mature OSNs	[2]
PGP9.5	Human PGP9.5 protein purified from pathogen free human brain	Cedarlane (RA95101)	AB_2313685	Rabbit	1:7,000 2°	OSNs	[1] (Holbrook et al., 2011)
SOX2	Transcription factor Sox2	Invitrogen (14-9811-82)	AB_11219471	Rat	1:300 2°	Upstream GBCs, HBCs, sus cells	[1] (Child et al., 2018)
SOX9	KLH-conjugated to the C-terminal sequence of human Sox9	Emd Millipore (AB5535)	AB_2239761	Rabbit	1:100 2°	Duct cells, gland cells	[1] (Holbrook et al., 2011)
TBX21	Synthetic peptide within Human T-bet/ Tbx21 aa 1-100 (N terminal)	Abcam (ab150440)	AB_2889209	Rabbit	1:500 3° (adult) TSA (fetal)	Mitral cells	[1] (Child et al., 2018)
TBX21	Full length recombinant mouse T-bet	Abcam (ab91109)	AB_2050371	Mouse	1:100 3° (adult) TSA (fetal)	Mitral cells	[2]
TUJ1	Rat brain derived microtubules	BioLegend (MMS-435P-250)	AB_2313773	Mouse	1:1000 1:2000 (WM) 2°	OSNs	[1] (Holbrook et al., 2011)
TH	SDS-denatured rat tyrosine hydroxylase	Invitrogen (P21962)	AB_2539844	Rabbit	1:1000 3° (adult) TSA (fetal)	Dopaminergic periglomerular cells	[2]
TH	Shared regions of the Tyroxine Hydroxylase gene product between human and mouse	Abcam (ab76442)	AB_1524535	Chicken	1:300 3° (adult) TSA (fetal)	Dopaminergic periglomerular cells	[2]
VGLUT2	C-terminal region of Mouse VGLUT2 conjugated to KLH	Abcam (ab84103)	AB_10674784	Rabbit	1:500 3°	Synaptic terminals of OSNs in OB glomeruli	[2]

Abbreviations: **GBCs –** global basal cells; **HBCs –** horizontal basal cells; **OB –** olfactory bulb; **OMP –** olfactory marker protein; **OSNs –** olfactory sensory neurons; **RE –** respiratory epithelium; **TH –** tyrosin hydroxylase; **TSA –** tyramide signal amplification; **TUJ1 –** ß-tubulin III; **VGLUT2 –** vesicular glutamate transporter type 2; **WM –** whole mount; [1] - prior published report; [2] - specificity based on known cell type expression of protein and absence of staining with removal of antibody